Cell Reports

Article

GABAergic disinhibition from the BNST to PNOC^{ARC} neurons promotes HFD-induced hyperphagia

Graphical abstract

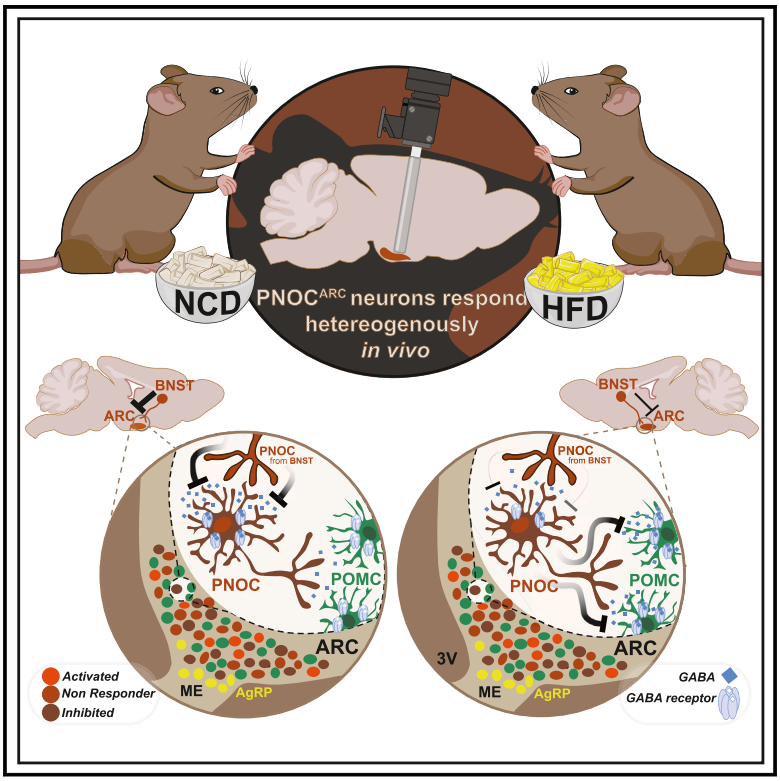

Highlights

- PNOC^{ARC} neurons are responsible for increased inhibition of POMC neurons upon HFD feeding
- A subpopulation of PNOC^{ARC} neurons is inhibited upon gastrointestinal nutrient sensing
- PNOC^{ARC} neuron activity increases upon HFD feeding through a disinhibitory mechanism
- HFD feeding weakens inhibitory input from PNOC^{BNST} neurons to PNOC^{ARC} neurons

Authors

Tamara Sotelo-Hitschfeld, Marielle Minère, Paul Klemm, ..., Peter Kloppenburg, Henning Fenselau, Jens Claus Brüning

Correspondence

henning.fenselau@sf.mpg.de (H.F.), bruening@sf.mpg.de (J.C.B.)

In brief

Sotelo-Hitschfeld et al. show in mice that overconsumption of high-caloric food is mediated through the disinhibition of a subpopulation of PNOC^{ARC} neurons. This disinhibition is facilitated through postsynaptic changes in the PNOC^{BNST} → PNOC^{ARC} circuit. Furthermore, physiological inhibition of PNOC^{ARC} neurons occurs upon nutrient sensing in the gut.

Sotelo-Hitschfeld et al., 2024, Cell Reports *43*, 114343
June 25, 2024
https://doi.org/10.1016/j.celrep.2024.114343

CellPress

Cell Reports

CellPress
OPEN ACCESS

Article

GABAergic disinhibition from the BNST to PNOC^{ARC} neurons promotes HFD-induced hyperphagia

Tamara Sotelo-Hitschfeld,[1,2,3,9] Marielle Minère,[2,4,9] Paul Klemm,[1,2,3] Diba Borgmann,[4,5] Daria Wnuk-Lipinski,[1,2,3] Alexander Jais,[1,2,3,6] Xianglian Jia,[1,2,3] Svenja Corneliussen,[1,3,7] Peter Kloppenburg,[3,7] Henning Fenselau,[2,3,4,*] and Jens Claus Brüning[1,8,10,*]

[1]Department of Neuronal Control of Metabolism, Max Planck Institute for Metabolism Research, Cologne, Germany
[2]Policlinic for Endocrinology, Diabetes, and Preventive Medicine (PEDP), University Hospital Cologne, Kerpener Strasse 26, 50924 Cologne, Germany
[3]Excellence Cluster on Cellular Stress Responses in Aging Associated Diseases (CECAD) and Center of Molecular Medicine Cologne (CMMC), University of Cologne, Joseph-Stelzmann-Strasse 26, 50931 Cologne, Germany
[4]Synaptic Transmission in Energy Homeostasis Research Group, Max Planck Institute for Metabolism Research, Cologne, Germany
[5]Novo Nordisk Foundation Center for Basic Metabolic Research, Faculty of Health and Medical Sciences, University of Copenhagen, Copenhagen, Denmark
[6]Helmholtz Institute for Metabolic, Obesity and Vascular Research (HI-MAG) of the Helmholtz Zentrum München at the University of Leipzig and University Hospital Leipzig, Leipzig, Germany
[7]Institute of Zoology, Faculty of Mathematics and Natural Sciences, University of Cologne, Cologne, Germany
[8]National Center for Diabetes Research (DZD), Ingolstädter Landstrasse 1, 85764 Neuherberg, Germany
[9]These authors contributed equally
[10]Lead contact
*Correspondence: henning.fenselau@sf.mpg.de (H.F.), bruening@sf.mpg.de (J.C.B.)
https://doi.org/10.1016/j.celrep.2024.114343

SUMMARY

Activation of prepronociceptin (PNOC)-expressing neurons in the arcuate nucleus (ARC) promotes high-fat-diet (HFD)-induced hyperphagia. In turn, PNOC^{ARC} neurons can inhibit the anorexic response of proopiomelanocortin (POMC) neurons. Here, we validate the necessity of PNOC^{ARC} activity for HFD-induced inhibition of POMC neurons in mice and find that PNOC^{ARC}-neuron-dependent inhibition of POMC neurons is mediated by gamma-aminobutyric acid (GABA) release. When monitoring individual PNOC^{ARC} neuron activity via Ca^{2+} imaging, we find a subpopulation of PNOC^{ARC} neurons that is inhibited upon gastrointestinal calorie sensing and disinhibited upon HFD feeding. Combining retrograde rabies tracing and circuit mapping, we find that PNOC neurons from the bed nucleus of the stria terminalis (PNOC^{BNST}) provide inhibitory input to PNOC^{ARC} neurons, and this inhibitory input is blunted upon HFD feeding. This work sheds light on how an increase in caloric content of the diet can rewire a neuronal circuit, paving the way to overconsumption and obesity development.

INTRODUCTION

Obesity and obesity-related disorders continue to rise in society, reducing both the length and the quality of life. A leading cause of the increase in obesity is the overconsumption of foods high in sugars and fats, foods that have also increased in availability.[1] Understanding the neurobiological mechanism(s) responsible for hyperphagia in response to highly caloric foods can thus become key for devising new strategies to fight obesity. Within the central nervous system (CNS), regulation of feeding, glucose homeostasis, and insulin sensitivity are orchestrated in the hypothalamus.[2] Over the past years, research has primarily focused on two separate populations residing in the arcuate nucleus (ARC) marked by the expression of agouti-related peptide (AgRP) and proopiomelanocortin (POMC).[3] Activated AgRP neurons release AgRP, neuropeptide Y (NPY), and gamma-aminobutyric acid (GABA) to downstream sites to promote feeding.[3–6] However, POMC neuron activity leads to the release of alpha-melanocyte-stimulating hormone (α-MSH) from their terminals, which induces satiety through melanocortin receptor activation in the paraventricular nucleus of the hypothalamus (PVH).[7–9] The activation of both AgRP and POMC neurons is regulated through changes in circulating cues such as leptin and ghrelin as well as modifications in neuronal input and signals from the gastrointestinal tract.[2] Moreover, recent work has shown that sensory perception of food alone can rapidly modulate their activity levels[10–12] and adapt protein-folding capacity and mitochondrial function in the liver.[13,14] Together, these two neuronal populations are key in orchestrating homeostatic feeding responses. However, this homeostatic regulation is disrupted

when animals are exposed to a palatable high-fat diet (HFD), even if AgRP neurons are ablated,[15] indicating that obesity can develop in the absence of these important orexigenic neurons. We have recently identified a population of ARC cells, characterized by prepronociceptin (PNOC) expression, which are rapidly activated upon HFD consumption.[16] Strikingly, in contrast to what is observed upon AgRP neuron ablation, ablation of PNOC^{ARC} neurons blunts HFD-induced body weight gain and hyperphagia.[16]

PNOC^{ARC} neurons represent a distinct, yet molecularly heterogeneous, orexigenic population that forms strong GABAergic inhibitory connections to POMC neurons.[16,17] To further define the role and regulation of PNOC^{ARC} neurons during obesity development, we (1) investigated the necessity of PNOC^{ARC} neuron activity for HFD-induced POMC neuron inhibition, (2) evaluated the contribution of GABA and nociceptin neurotransmitter release from PNOC^{ARC} neurons to the acute HFD-induced POMC inhibition and hyperphagia, (3) characterized the physiological feeding-related regulators of PNOC^{ARC} activity *in vivo*, and (4) identified the mechanism that drives the increase in PNOC^{ARC} activity upon acute HFD feeding.

RESULTS

PNOC^{ARC} neurons are required for HFD-induced POMC neuron inhibition

We previously identified that 3 days of HFD (3dHFD) feeding activates PNOC^{ARC} neurons, which is paralleled by an increase in the inhibitory, GABAergic tone on POMC neurons.[16] To directly test whether the 3dHFD-induced activation of PNOC^{ARC} neurons is responsible for this increase in POMC neuron inhibition, we acutely silenced PNOC^{ARC} neurons while determining the inhibitory GABAergic input to POMC neurons. We injected adeno-associated viruses (AAVs) expressing a Cre-dependent chemogenetic inhibitory receptor construct (AAV-FLEX-hM4Di-mCherry) into the ARC of *PNOC-Cre::POMC-eGFP* mice, followed by preparation of brain slices to record spontaneous inhibitory postsynaptic currents (sIPSCs) from GFP-labeled POMC neurons (Figures 1A and 1B). sIPSCs were recorded from POMC neurons in brain slices under control conditions and after incubation (>1 h) with the hM4Di actuator clozapine *N*-oxide in unpaired recordings (CNO; 10 μM; Figures 1C–1E). In addition, the acute effects of PNOC^{ARC} neuron silencing on sIPSCs were assessed through wash-in of CNO in paired recordings (Figure 1F). Corroborating our previous findings,[16] 3dHFD feeding evoked a trend toward an increase in the sIPSC frequency in POMC neurons (Figure 1E, 2.76 ± 0.81 Hz [normal chow diet, NCD] versus 5.02 ± 1.11 Hz [3dHFD]). Incubation of brain slices from 3dHFD-fed mice with CNO reduced the sIPSC frequency (Figure 1E, 5.02 ± 1.11 Hz [3dHFD] versus 1.93 ± 0.3 Hz [3dHFD + CNO]) to what we observed under NCD control conditions (Figure 1E, 2.76 ± 0.81 Hz [NCD] versus 1.93 ± 0.3 Hz [3dHFD + CNO]). In addition, we observed that the acute CNO/hM4Di-induced inhibition of PNOC^{ARC} neurons reduced the frequency of sIPSCs recorded from POMC neurons in brain slices from mice that were exposed to the 3dHFD protocol (Figure 1F, 3.43 ± 0.39 Hz [3dHFD] versus 1.68 ± 0.16 Hz [3dHFD + CNO]). Remarkably, CNO administration failed to decrease the sIPSC frequency recorded from POMC neurons in brain slices from control NCD-fed mice (Figure 1E, 2.76 ± 0.81 Hz [NCD] versus 2.67 ± 0.58 Hz [NCD + CNO]; Figure 1F, 1.94 ± 0.56 Hz [NCD] versus 1.47 ± 0.32 Hz [NCD + CNO]), suggesting that PNOC^{ARC} neurons do not contribute to the basal inhibitory tone of POMC neurons. Thus, increased PNOC^{ARC} neuron activity mediates the increased inhibitory tone to POMC neurons upon acute 3dHFD exposure.

Nociceptin silences POMC neurons

In addition to GABA, PNOC^{ARC} neurons can modulate innervated neurons through the release of the neuropeptide nociceptin (product of the *Pnoc* gene).[18] To test the ability of nociceptin to regulate POMC neuron activity, we performed perforated patch-clamp recordings from GFP-expressing POMC neurons in *POMC-eGFP* mice (Figure S1A). *Post hoc*, the identity of the recorded neurons was confirmed by double labeling with biocytin and eGFP (Figure S1B). Current-clamp recordings revealed a concentration-dependent decrease in action potential frequency as well as an increase in hyperpolarization during bath application with increasing concentrations of nociceptin (1, 10, 100, and 500 nM; n = 5, Figure S1C). At 1 nM, the mean action potential frequency decreased from 2.6 ± 0.4 to 2.2 ± 0.5 Hz. At 10 nM, all recorded neurons ceased firing, hyperpolarizing by ΔE_M = 11.4 ± 4.8 mV. An increase in the nociceptin concentration to 100–500 nM further enhanced hyperpolarization (at 500 nM, ΔE_M = 24.5 ± 5.2 mV) (Figure S1D).

To better understand the concentration-dependent effects of nociceptin, we next performed voltage-clamp measurements from a holding potential of −55 mV using finer gradations of nociceptin concentration (1, 3, 6, 10, 50, and 100 nM; n = 5, Figures S1E and S1F). The nociceptin-induced currents (I_{noc}) activated at a concentration of ∼1 nM and had an EC_{50} of 25.4 nM (95% CI 15.8–74.2 nM, sigmoidal dose-response fit). The maximum amplitude determined from the sigmoidal fit was $I_{noc,max}$ = 39.2 ± 7.1 pA. Given the mean whole-cell capacity of C_M = 20.0 ± 2.8 pF, this corresponds to a current density of 2.3 ± 0.3 pA pF^{-1}. Taken together, these data show that even low concentrations of nociceptin can be effective in inhibiting POMC neurons and suggest that PNOC^{ARC} neurons can potently inhibit POMC neurons through the release of nociceptin.

Nociceptin is not required for PNOC^{ARC} neuron-induced hyperphagia

Because PNOC^{ARC} neurons express characterized inhibitors of POMC neurons, i.e., GABA and nociceptin, we next investigated the contribution of nociceptin from PNOC^{ARC} neurons to promote hyperphagia, in addition to that of GABA,[16] by optogenetically stimulating PNOC^{ARC} neurons in mice that lack the ability to produce nociceptin (PNOC$^{Cre/Cre}$; Figure 2A). Given that the cDNA of the Cre recombinase is introduced into exon 2 of the *Pnoc* gene in our *Pnoc-Cre* mouse model, the presence of the Cre insertion prevents transcription and expression of the *Pnoc* gene. In heterozygosity (*PNOC*$^{Cre/+}$), mice express both nociceptin and Cre recombinase, from either one of the alleles of the *Pnoc* gene. Homozygous *PNOC-Cre* (PNOC$^{Cre/Cre}$) mice, however, do not express nociceptin, as both *Pnoc* gene alleles

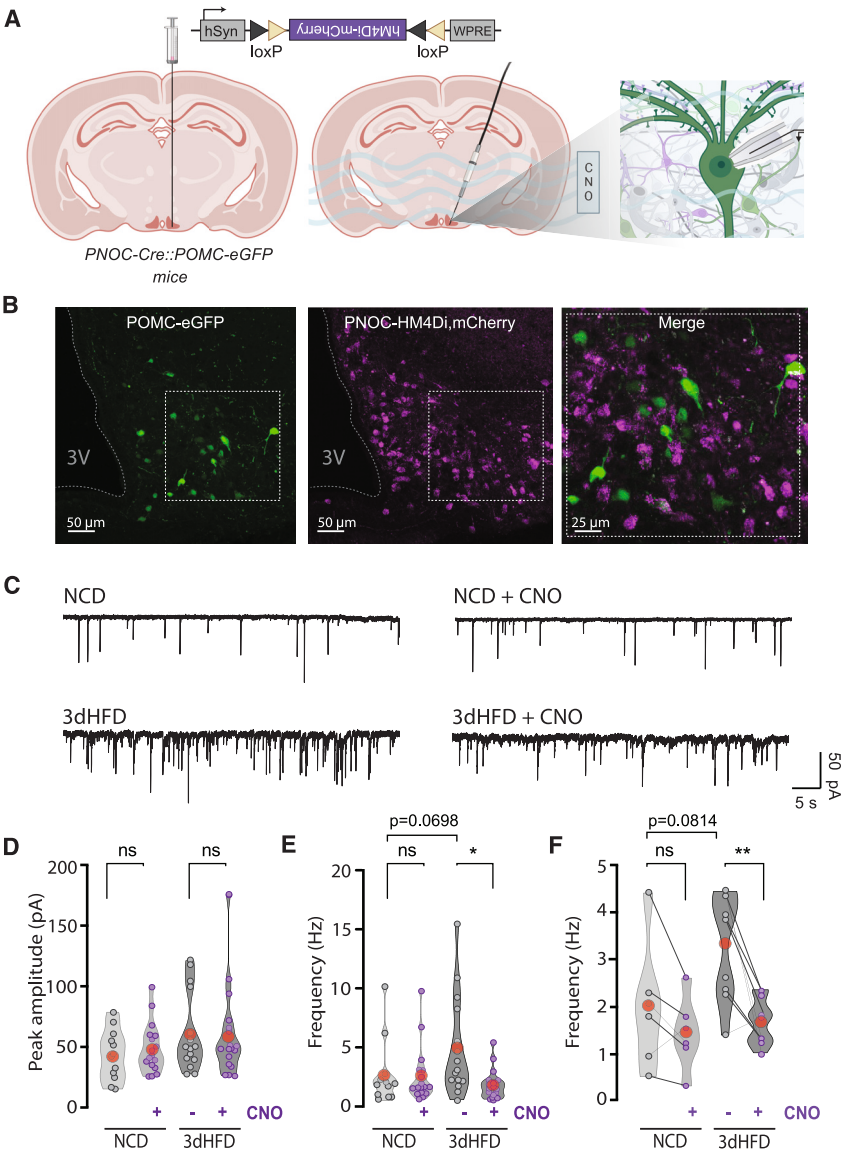

Figure 1. PNOC^{ARC} neuron activation accounts for HFD-induced inhibition of POMC neurons

(A) Experimental design: AAV-hSyn-DIO-HM4Di-mCherry was injected into the ARC of *PNOC-Cre::POMC-eGFP* mice. Following acute brain slice preparation, spontaneous inhibitory postsynaptic currents (sIPSCs) were recorded from POMC neurons (visualized by eGFP) at baseline and after bath application of CNO (10μM) to inhibit hM4D-expressing PNOC^{ARC} neurons.

(B) Example images of eGFP expression in POMC neurons (left, green; scale bar, 50 μm) and Cre-dependent expression of hM4Di-mCherry (middle, magenta; scale bar, 50 μm) in PNOC^{ARC} neurons in *PNOC-Cre::POMC-eGFP* mice. Right image shows a merge of both eGFP and hM4Di expression in the indicated area (scale bar, 25 μm).

(C–E) Example traces (C), peak amplitude (D), and frequency analyses (E) of sIPSCs recorded from POMC neurons at baseline and after bath incubation of CNO (10 μM) in brain slices from NCD and 3dHFD mice. (D) NCD: 43.4 ± 5.95 pA. NCD + CNO: 48.9 ± 4.9 pA. 3dHFD: 61.6 ± 8.4 pA. 3dHFD + CNO: 59 ± 8.6 pA. (E) NCD: 2.76 ± 0.81 Hz. NCD + CNO: 2.67 ± 0.58 Hz. 3dHFD: 5.02 ± 1.11 Hz. 3dHFD + CNO: 1.93 ± 0.3 Hz. Number of mice: 3 (NCD), 3 (NCD + CNO), 3 (3dHFD), and 3 (3dHFD + CNO). Number of cells: 12 (NCD), 15 (NCD + CNO), 17 (3dHFD), and 18 (3dHFD + CNO).

(F) Frequency analysis of sIPSCs at baseline and after acute bath application of CNO (10 μM) in brain slices from NCD and 3dHFD mice. NCD: 2.04 ± 0.56 Hz. NCD + CNO: 1.47 ± 0.32 Hz. 3dHFD: 3.43 ± 0.39 Hz. 3dHFD + CNO: 1.68 ± 0.16 Hz. Number of mice: 2 (NCD/NCD + CNO) and 2 (3dHFD/3dHFD + CNO). Number of cells: 6 (NCD/NCD + CNO) and 12 (3dHFD/3dHFD + CNO). Statistical analyses were performed by two-way ANOVA followed by Tukey's *post hoc* test (D and E) and both paired and unpaired two-tailed Student's t tests (F). ns, not significant; $^{*}p \leq 0.05$, $^{**}p \leq 0.01$.

are disrupted, creating PNOC-knockout mice. To confirm our genetic nociceptin-knockout model, we determined *Cre* and *Pnoc* expression using *in situ* hybridization (ISH) (Figures S2A–S2C). Homozygous *PNOC-Cre* (PNOC$^{Cre/Cre}$) mice lacked expression of *Pnoc* in the ARC (Figures S2A and S2B, 57 ± 3 neurons [wild type, WT] versus 0 ± 0 neurons [PNOC$^{Cre/Cre}$]), while the expression of *Cre* in PNOC$^{Cre/Cre}$ mice was similar to that observed in PNOC$^{Cre/+}$ mice (Figures S2A and S2C, 50 ± 3 neurons [PNOC$^{Cre/+}$] versus 44 ± 3 neurons [PNOC$^{Cre/Cre}$]). In addition, PNOC$^{Cre/+}$ mice showed no difference in the number of *Pnoc*$^{+}$ neurons in the ARC compared to WT controls (Figures S2A and S2B, 53 ± 3 neurons [PNOC$^{Cre/+}$] versus 57 ± 3 neurons [WT]), whereas WT mice displayed an absence of *Cre* expression (Figures S2A and S2C, 0 ± 0 neurons [WT] versus 50 ± 3 neurons [PNOC$^{Cre/+}$]), confirming our Cre-dependent targeting approach of PNOC^{ARC} neurons in both nociceptin-producing (PNOC$^{Cre/+}$) and nociceptin-knockout (PNOC$^{Cre/Cre}$) genetic models.

To activate PNOC^{ARC} neurons that lack nociceptin, we expressed a Cre-dependent Channelrhodopsin-2 (ChR2) in the ARC of PNOC$^{Cre/Cre}$ mice (Figure 2A). Heterozygous littermates (PNOC$^{Cre/+}$) served as controls, enabling Cre-dependent ChR2 expression in PNOC^{ARC} neurons that retained nociceptin production from the remaining *Pnoc* WT allele (Figures S2A and S2C). As previously reported, optogenetic stimulation of PNOC^{ARC} neurons (20 Hz, 5 ms pulse, 1 s ON-3 s OFF) in PNOC$^{Cre/+}$ mice increased food intake (Figure 2B, 4.2 ± 0.47 g [laser OFF] versus 6.2 ± 0.43 g [laser ON]), while we had previously shown that the same stimulation protocol failed to increase food intake in control mice lacking ChR2-expression.[16] While PNOC$^{Cre/Cre}$ mice exhibited a slight reduction in food intake in the absence of laser stimulation (Figure 2B, 4.2 ± 0.47 g

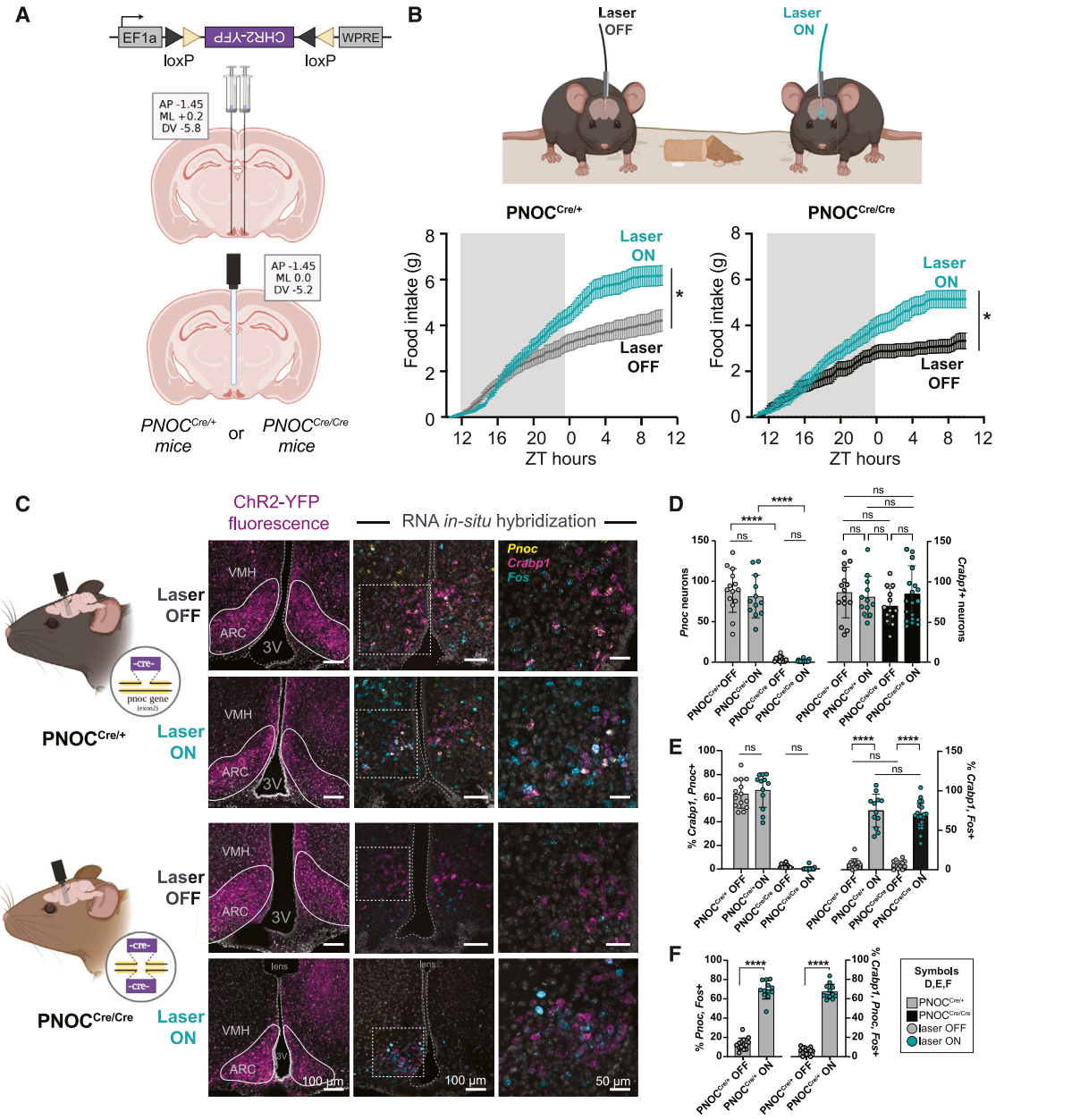

Figure 2. Nociceptin does not control hyperphagia in response to optogenetic PNOC^{ARC} neuron activation

(A) Experimental design: Cre-dependent expression of ChR2-EYFP in PNOC^{ARC} neurons (top) and optical fiber implantation above the ARC (bottom). The *PNOC-Cre* mouse line carries the Cre cDNA in exon 2 of the *Pnoc* gene.[16] Homozygous *PNOC-Cre* mice (PNOC$^{Cre/Cre}$) lack the *Pnoc* gene product.

(B) Normal chow diet (NCD) intake measurement for 24 h (ZT refers to zeitgeber time) at baseline (black, laser OFF) and during optogenetic stimulation (cyan, laser ON) of PNOC^{ARC} neurons in PNOC$^{Cre/+}$ (left; n = 9) and PNOC$^{Cre/Cre}$ (right; n = 7) mice. PNOC$^{Cre/+}$ laser OFF: 4.22 ± 1.4 g. PNOC$^{Cre/+}$ laser ON: 6.18 ± 1.3 g. PNOC$^{Cre/Cre}$ laser OFF: 3.33 ± 0.84 g. PNOC$^{Cre/Cre}$ laser ON: 5.15 ± 0.93 g.

(C) Histological validation of the optogenetic stimulation of PNOC^{ARC} neurons. Left column: EYFP native fluorescence (magenta) in the ARC, representing ChR2 expression in PNOC^{ARC} neurons (scale bars, 100 µm). Middle column: ISH for *Pnoc* (yellow), *Crabp1* (magenta), and *fos* (cyan) (scale bars, 100 µm). Right column: higher-resolution images showing colocalization of detected signals of ISH (scale bars, 50 µm). To determine activated PNOC neurons in PNOC$^{Cre/Cre}$ mice, *Crabp1* and *cFos* expression was used. Laser ON indicates 1 h of photostimulation prior to sacrifice; laser OFF acts as unstimulated controls.

(D) Total number of *Pnoc*$^{+}$ (left) and *Crabp1*$^{+}$ cells (right). Left: *Pnoc*: PNOC$^{Cre/+}$ laser OFF, 88.15 ± 27 cells; PNOC$^{Cre/+}$ laser ON, 80 ± 26 cells; PNOC$^{Cre/Cre}$ laser OFF, 3 ± 3.2 cells; and PNOC$^{Cre/Cre}$ laser ON, 0.6 ± 1.3 cells. Right: *Crabp1*$^{+}$: PNOC$^{Cre/+}$ laser OFF, 85.3 ± 31.4 cells; PNOC$^{Cre/+}$ laser ON, 80.2 ± 25.5 cells; PNOC$^{Cre/Cre}$ laser OFF, 68.5 ± 22 cells; and PNOC$^{Cre/Cre}$ laser ON, 84.9 ± 34.8 cells. Number of brain slices: 14 (PNOC$^{Cre/+}$, laser OFF), 12 (PNOC$^{Cre/+}$, laser ON), 13 (PNOC$^{Cre/Cre}$, laser OFF), and 20 (PNOC$^{Cre/Cre}$, laser ON). Number of mice: 5 (PNOC$^{Cre/+}$) and 4 (PNOC$^{Cre/Cre}$).

(E) Percentage of *Crabp1*$^{+}$ cells expressing *Pnoc* (left) or *Crabp1*$^{+}$ cells expressing *cFos* (right). Left: *Pnoc*$^{+}$*Crabp*$^{+}$: PNOC$^{Cre/+}$ laser OFF, 63.11% ± 12.1%; PNOC$^{Cre/+}$ laser ON, 66.1% ± 14.5%; PNOC$^{Cre/Cre}$ laser OFF, 0.6% ± 1.5%; and PNOC$^{Cre/Cre}$ laser ON, 0.35% ± 1.21%. Right: *Crabp1*$^{+}$*Fos*$^{+}$: PNOC$^{Cre/+}$ laser

(legend continued on next page)

[PNOC$^{Cre/+}$] versus 3.3 ± 0.3 g [PNOC$^{Cre/Cre}$]), they retained the ability to mount a hyperphagic response during optogenetic stimulation of PNOC^{ARC} neurons (Figure 2B, 3.3 ± 0.3 g [laser OFF] versus 5.1 ± 0.34 g [laser ON]). In addition, PNOC^{ARC} stimulation increased the respiratory quotient (RQ) during the light cycle (Figures S2D and S2E, PNOC$^{Cre/+}$, AUC 1.66 ± 0.6 [day, laser OFF] versus AUC 2.94 ± 0.70 [day, laser ON]; PNOC$^{Cre/Cre}$, 2.09 ± 0.76 [day, laser OFF] versus 3.23 ± 0.76 [day, laser ON]), consistent with increased caloric intake. We observed no differences in locomotion during optogenetic stimulation of PNOC^{ARC} neurons (Figures S2F and S2G). These findings demonstrate that nociceptin release from PNOC^{ARC} neurons is not required for the promotion of hyperphagia upon their activation.

We next aimed at validating the successful optogenetic activation of PNOC^{ARC} neurons in the presence and absence of functional PNOC expression using *Crabp1*, which is an alternative gene that marks a major subset of PNOC^{ARC} neurons[17] (Figures 2C–2F). PNOC$^{Cre/Cre}$ mice, despite an absence of *Pnoc* expression (3.3% ± 0.8% [PNOC$^{Cre/Cre}$, laser OFF], 0.6% ± 1.3% [PNOC$^{Cre/Cre}$, laser ON]), show equivalent numbers of *Crabp1*$^{+}$ cells compared with PNOC$^{Cre/+}$ mice (85% ± 31% [PNOC$^{Cre/+}$ OFF], 80% ± 25% [PNOC$^{Cre/+}$ ON], 69% ± 22% [PNOC$^{Cre/Cre}$ OFF], and 84% ± 35% [PNOC$^{Cre/Cre}$ ON]), confirming that *Crabp1*-expressing PNOC^{ARC} neurons are still present in PNOC$^{Cre/Cre}$ mice, and homozygosity for the Cre-recombinase in the PNOC$^{Cre/Cre}$ mice did not affect the expression of other endogenously expressed genes. To identify optogenetically activated PNOC^{ARC} neurons in PNOC$^{Cre/Cre}$ mice, we determined the expression of *cFos* mRNA in *Crabp1*-expressing cells of the ARC (Figures 2C–2F). Photostimulation of the ARC in ChR2-expressing PNOC$^{Cre/+}$ and PNOC$^{Cre/Cre}$ mice efficiently activated PNOC^{ARC} neurons as assessed by *cFos* expression in *Crabp1*$^{+}$ cells (Figure 2E, 8% ± 6% [PNOC$^{Cre/+}$ OFF] versus 75% ± 20% [PNOC$^{Cre/+}$ ON]; 7% ± 5% [PNOC$^{Cre/Cre}$ OFF] versus 68% ± 16% [PNOC$^{Cre/Cre}$ ON]).

To confirm that the activated *Crabp1*-expressing population corresponds to the target PNOC population, we further analyzed *cFos* mRNA expression in either *Pnoc*$^{+}$ or *Pnoc*$^{+}$*Crabp1*$^{+}$ neurons in the ARC of PNOC$^{Cre/+}$ mice and found identical numbers of activated neurons (Figure 2F, 69% ± 9% [*Pnoc*$^{+}$*cFos*$^{+}$, PNOC$^{Cre/+}$ ON] versus 67% ± 8% [*Pnoc*$^{+}$*Crabp1*$^{+}$*cFos*$^{+}$, PNOC$^{Cre/+}$ ON]. These results show that we effectively optogenetically activated PNOC^{ARC} neurons in mice lacking nociceptin expression.

A subcluster of PNOC^{ARC} neurons is disinhibited upon 3dHFD feeding

To elucidate the regulatory mechanisms of PNOC^{ARC} neuronal activity during 3dHFD feeding, we measured the activity of individual PNOC^{ARC} neurons *in vivo* using single-cell Ca^{2+} imaging with the Inscopix miniscope under various dietary stimuli. We expressed the cytosolic calcium sensor GCaMP6s in the ARC of PNOC$^{Cre/+}$ mice and implanted a gradient-index (GRIN) lens directly above the ARC (Figures 3A, 3B, and S3), enabling the recording of fluorescence changes in single PNOC^{ARC} neurons in mice exhibiting natural behaviors (Figure 3C). We first assessed how feeding affects PNOC^{ARC} neuron activity profiles in NCD- and 3dHFD-fed mice that were fasted overnight. Analysis of activity changes in individual PNOC^{ARC} neurons upon the presentation and consumption of a food pellet in NCD-fed mice revealed the presence of differentially regulated PNOC^{ARC} neuron clusters, with an activated cluster (UP), another subset that did not significantly change its activity (NON), and a third cluster of neurons that was inhibited (DOWN) (Figure 3D). Interestingly, while the refeeding-induced activity pattern of the activated and non-responder cell cluster did not change in 3dHFD mice compared to the NCD group, refeeding resulted in a less pronounced inhibition of the refeeding-inhibited cluster in 3dHFD mice (Figure 3G, UP, 3.4 ± 3.3 *Z* score [NCD] versus 3.85 ± 3.64 *Z* score [3dHFD]; NON, 0.15 ± 0.27 *Z* score [NCD] versus 0.14 ± 0.28 *Z* score [3dHFD]; DOWN, −0.95 ± 0.78 *Z* score [NCD] versus −0.56 ± 0.29 *Z* score [3dHFD]), without altering the total proportion of PNOC^{ARC} neurons that were inhibited (Figures 3E and 3F, 29% [NCD] versus 26.4% [3dHFD]). Thus, the activation of the overall PNOC^{ARC} population upon 3dHFD feeding occurs through a reduced inhibition of the inhibited (DOWN) subcluster of PNOC^{ARC} neurons.

To evaluate the importance of postingestive signaling in regulating PNOC^{ARC} activity, we implanted catheters into the stomach for the gastric infusion (GI) of a highly caloric solution (vanilla Ensure, 1.2 mL, 2.4 calories; Figure 4A). In animals fasted for 8 h, administration of Ensure into the stomach elicited heterogeneous responses in individual PNOC^{ARC} neurons in NCD-fed and 3dHFD-fed mice (Figures 4B and 4C, UP, 13% [NCD] versus 31.7% [3dHFD]; NON, 48.1% [NCD] versus 34.15% [3dHFD]; DOWN, 38.9% [NCD] versus 34.15% [3dHFD]). While we observed that Ensure infusion resulted in an overall decrease in PNOC^{ARC} neuron activity in both NCD- and 3dHFD-fed mice (Figure 4D, NCD baseline, 0.32 ± 0.5 *Z* score; GI, 0.12 ± 0.32 *Z* score; post GI, −0.24 ± 0.34 *Z* score. 3dHFD baseline, 0.082 ± 0.55 *Z* score; GI, 0.18 ± 0.45 *Z* score; post GI, −0.10 ± 0.35 *Z* score), the degree of inhibition caused by Ensure infusion was significantly blunted in 3dHFD-fed animals (Figure 4E, NCD, −0.57 ± 0.86 *Z* score; 3dHFD, −0.18 ± 0.84 *Z* score; Figure 4G, DOWN −2.30 ± 2.02 *Z* score [NCD] versus −1.18 ± 0.71 *Z* score [3dHFD]). Thus, the ability of postingestive

OFF, 7.7% ± 6.3%; PNOC$^{Cre/+}$ laser ON, 74.7% ± 20.9%; PNOC$^{Cre/Cre}$ laser OFF, 6.6% ± 5%; and PNOC$^{Cre/Cre}$ laser ON, 67.7% ± 15.9%. Number of brain slices: 14 (PNOC$^{Cre/+}$, laser OFF), 12 (PNOC$^{Cre/+}$, laser ON), 13 (PNOC$^{Cre/Cre}$, laser OFF), and 20 (PNOC$^{Cre/Cre}$, laser ON). Number of mice: 5 (PNOC$^{Cre/+}$) and 4 (PNOC$^{Cre/Cre}$).

(F) Percentage of *Pnoc*$^{+}$ cells expressing *cFos* (left) or *Crabp1*$^{+}$*Pnoc*$^{+}$ cells expressing *cFos* (right) in PNOC$^{Cre/+}$ mice. Left: *Pnoc*$^{+}$*Fos*$^{+}$: PNOC$^{Cre/+}$ laser OFF, 12.6% ± 6%, and PNOC$^{Cre/+}$ laser ON, 69.4% ± 9.4%. Right: *Crabp1*$^{+}$*Pnoc*$^{+}$*Fos*$^{+}$: PNOC$^{Cre/+}$ laser OFF, 5.7% ± 3.7%, and PNOC$^{Cre/+}$ laser ON, 67% ± 7.6%. Number of brain slices: 14 (laser OFF) and 12 (laser ON). Number of mice: 5. Data are represented as the mean ± SEM. Statistical analysis was performed using two-way ANOVA followed by Tukey's *post hoc* test (B) and one-way ANOVA by Šídák test (D). ns, not significant; ****$p \leq 0.0001$.

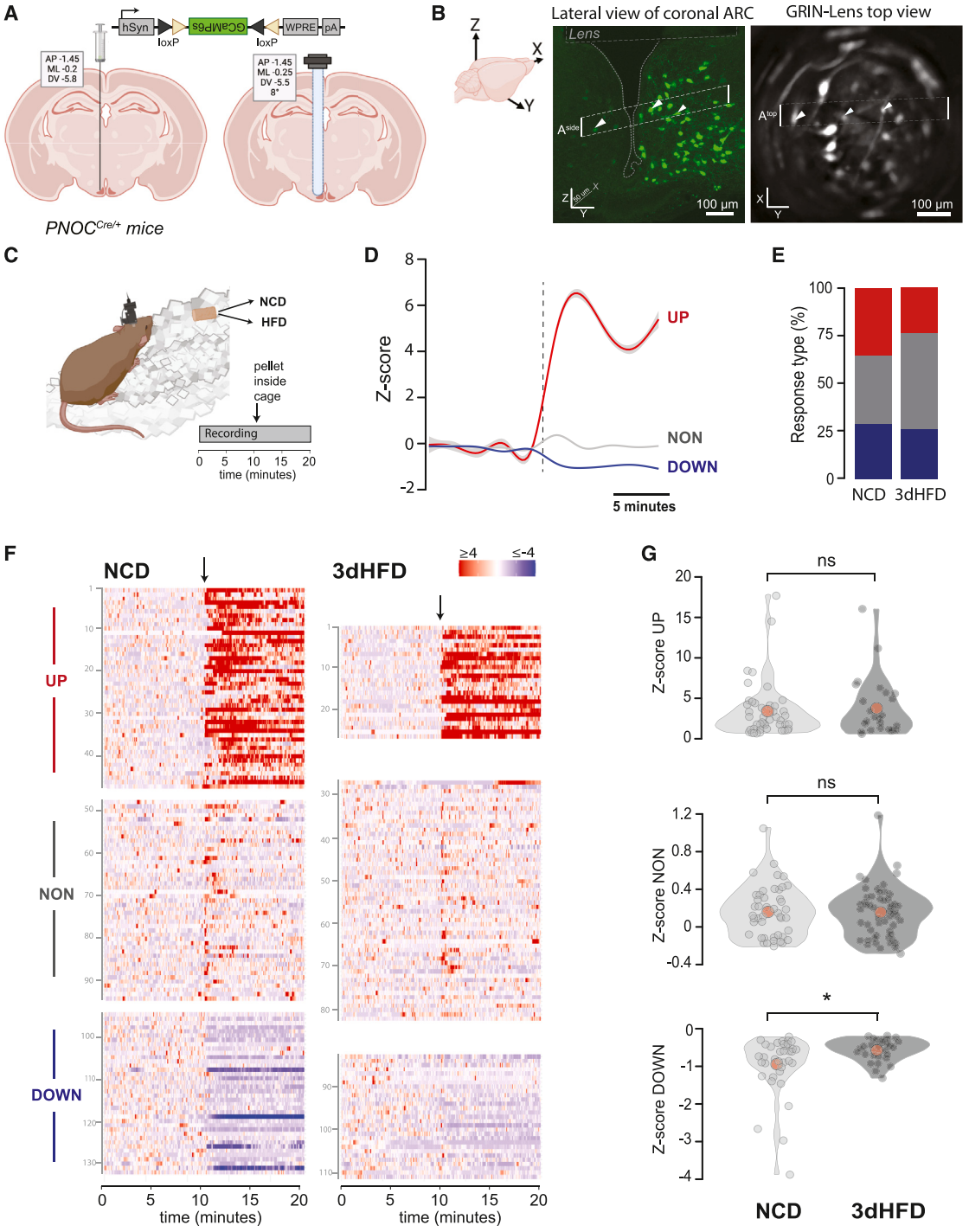

Figure 3. PNOC^{ARC} neurons exhibit heterogeneous responses and are disinhibited after 3dHFD feeding

(A) Schematic for unilateral *AAV1-hSyn-FLEX-GCaMP6s* virus injection and GRIN-lens implantation.

(B) Anatomical identification of recorded PNOC neurons. Left: mouse brain. Axes represent X, anterior-posterior (AP); Y, medial-lateral (ML); and Z, dorsal-ventral (DV). Middle: tissue containing lens above the arcuate was divided into nine coronal sections from anterior to posterior (X1, …, X9) of 50 μm thickness each. Here, the middle section of the lens is shown (X5). Lateral view of the coronal ARC shows GCaMP6s expression in PNOC neurons and A^{side} box represents the focal plane of the miniscope (scale bar, 100 μm). Right: miniscope FOV (field of view) corresponds to neuronal view at Z lens depth. A^{top} box shows neurons found in slice X5 at the A^{side} box view. Matching neurons are indicated with arrowheads (scale bar, 100 μm). Extended explanation can be found in Figure S3.

(C) Experimental design: after 16 h of fasting, mice were attached to the camera in their home cage. The recording protocol was 10 min of baseline and 10 min after a chow pellet was presented.

(legend continued on next page)

signaling to inhibit PNOC^{ARC} neurons is blunted after 3dHFD exposure.

HFD feeding reduces synaptic inhibition of PNOC^{ARC} neurons

We previously found that the intrinsic excitability of PNOC^{ARC} neurons increases upon 3dHFD feeding.[16] These cell-intrinsic changes may contribute to the observed impairment of PNOC^{ARC} neuron inhibition upon GI of Ensure in 3dHFD-fed animals. In addition, 3dHFD-induced modifications in the synaptic inputs to PNOC^{ARC} from upstream sites may contribute to their altered acute activity state. To test the latter possibility, we systematically evaluated changes in the excitatory and inhibitory synaptic inputs to PNOC^{ARC} neurons by recording spontaneous excitatory postsynaptic currents (sEPSCs) and sIPSCs from eGFP-expressing neurons in the ARC of *PNOC-eGFP* mice exposed to either NCD or 3dHFD (Figure 5A). We found that 3dHFD did not change sEPSC amplitude (Figure 5B, 16.13 ± 1.5 pA [NCD] versus 13.67 ± 3.27 pA [3dHFD]) or frequency (Figure 5B, 2.06 ± 0.51 Hz [NCD] versus 1.45 ± 0.39 Hz [3dHFD]), whereas we observed a profound reduction in the amplitude (50.84 ± 6.35 pA [NCD] versus 35.2 ± 3.26 pA [3dHFD]) and frequency (2.71 ± 0.48 Hz [NCD] versus 1.3 ± 0.18 Hz [3dHFD]) of sIPSCs in PNOC^{ARC} neurons (Figure 5C). Thus, acute HFD reduces the spontaneous inhibitory tone on PNOC^{ARC} neurons, raising the possibility that disinhibition is a key aspect modulating PNOC^{ARC} neuron responses to gut-derived signals during obesity development.

PNOC^{ARC} neurons receive strong GABAergic input from the BNST

Upstream brain sites could be responsible for gut-signal-derived inhibition of these neurons and could be modulated upon 3dHFD feeding. To identify GABAergic input to PNOC^{ARC} neurons, we used EnvA-pseudotyped G-deleted rabies mapping to define areas that provide monosynaptic afferents of PNOC^{ARC} neurons using PNOC$^{Cre/+}$ mice (Figures 5D–5F and S4A). Our analysis revealed that PNOC^{ARC} neurons receive inputs from nearby ARC neurons as well as from other brain regions that are linked to the regulation of energy balance, including the PVH (15.8% ± 3.8%), lateral hypothalamus (LH; 11.4% ± 4.1%), dorsomedial hypothalamus (DMH; 6.49% ± 1.72%), ventromedial hypothalamus (VMH; 6.12% ± 1.72%), medial preoptic nucleus (MPO; 7.35% ± 4.3%), supraoptic nucleus (SON; 5.5% ± 1.1%), retrochiasmatic area (RCh; 1.6% ± 1.2%), zona inserta (ZI; 0.98% ± 0.3%), and bed nucleus of the stria terminalis (BNST; 2.98% ± 1.79%) (Figures S4B–S4D). Of interest, these input areas of PNOC^{ARC} neurons show a high overlap with those of both POMC and AgRP neurons,[19] underpinning an intense regulatory input integration of PNOC^{ARC} neurons in the control of energy intake.

Based on our rabies mapping experiments, we next sought to identify which of the upstream sites could mediate the GABAergic disinhibition of PNOC^{ARC} neurons upon acute HFD feeding. One candidate input area is the BNST (Figure 5F), as it showed a high number of rabies-labeled neurons and is known for containing almost only GABAergic neurons.[20] In addition, the BNST receives input from hindbrain regions[21] that relay gut-derived information, potentially enabling the BNST to transmit postingestive information to PNOC^{ARC} neurons. We next assessed how 3dHFD feeding affects GABAergic synaptic transmission between BNST and PNOC^{ARC} neurons. As the BNST is a heterogeneous region,[22,23] we performed an in-depth topographical mapping of BNST inputs to PNOC^{ARC} neurons and found that rabies-infected neurons were detectable throughout the BNST (Figure S4E). Hence, we expressed ChR2 throughout the BNST of *PNOC-eGFP* mice and recorded light-evoked inhibitory postsynaptic currents (le-IPSCs) from GFP-expressing PNOC^{ARC} neurons in brain slices from NCD- and 3dHFD-fed mice (Figures 6A and 6B). Optogenetic stimulation of BNST terminals elicited large-amplitude le-IPSCs that were completely blocked by adding the GABA-A receptor antagonist bicuculline (BIC) to the bath solution (Figure 6C, 104.10 ± 51.43 pA [control] versus 7.05 ± 1.58 pA [BIC]), confirming the existence of strong GABAergic connections between BNST and PNOC^{ARC} neurons. In mice from both NCD and 3dHFD feeding conditions, we observed that the vast majority of PNOC^{ARC} neurons received GABAergic input from the BNST, characterized by a high connectivity rate for both groups (89% [NCD] and 75% [3dHFD]; Figures 6D and 6E). Remarkably, 3dHFD feeding profoundly attenuated the amplitudes of the le-IPSCs recorded from PNOC^{ARC} neurons in mice expressing ChR2 in the BNST (Figures 6D and 6F, 452.3 ± 49.2 pA [NCD] versus 251.4 ± 42.9 pA [3dHFD]), reducing the effective inhibition through the BNST → PNOC^{ARC} circuit.

To determine whether this weakening of transmission across BNST → PNOC^{ARC} neuron synapses was due to variances in the release probability of GABA from axonal terminals or due to postsynaptic alterations of GABA-A receptors, we determined the decay kinetics as well as the paired pulse ratio (PPR) of le-IPSCs. We found that 3dHFD feeding evoked an increase in the decay time of le-IPSCs (Figure 6G, 24.6 ± 1.12 ms [NCD] versus 31.0 ± 1.49 ms [3dHFD]), without any obvious changes

(D) All neurons were normalized to their own baseline (*Z* score) and partitioned into three groups using K-means clustering. Color code: red, increased firing or activation (UP, 71 neurons); gray, non-responders (NON, 103 neurons); and blue, reduced firing or inhibition (DOWN, 67 neurons). Number of mice: 7.

(E) Percentage of neurons per cluster in the context of NCD (131 neurons) or 3dHFD (110 neurons). Red, activation; gray, non-responder; blue, inhibition.

(F) *Z* score traces of single PNOC neurons were separated by cluster and diet. *Z* score values $4 \geq 0 \leq -4$ represent activation < no response < inhibited. *Z* scores are delimited at ±4 for better visualization of the heatmap. NCD: 46 neurons UP, 47 neurons NON, 38 neurons DOWN. 3dHFD: 25 neurons UP, 56 neurons NON, 29 neurons DOWN.

(G) Mean of *Z* score after pellet presentation and separated by cluster. 3dHFD reduces the degree of inhibition of the inhibited cluster. UP, NCD, 3.35 ± 3.34 *Z* score. UP, 3dHFD, 3.86 ± 3.6 *Z* score. NON, NCD, 0.15 ± 0.27 *Z* score. NON, 3dHFD, 0.16 ± 0.29 *Z* score. DOWN, NCD, −0.95 ± 0.78 *Z* score. DOWN, 3dHFD, −0.6 ± 0.29 *Z* score. UP, activated; NON, non-responder; DOWN, inhibited. NCD: 46 neurons UP, 47 neurons NON, 38 neurons DOWN. 3dHFD: 25 neurons UP, 56 neurons NON, 29 neurons DOWN. Statistical analysis was performed using Fisher's exact test (E) and Welch's t test (G). ns, not significant; $^{*}p \leq 0.05$.

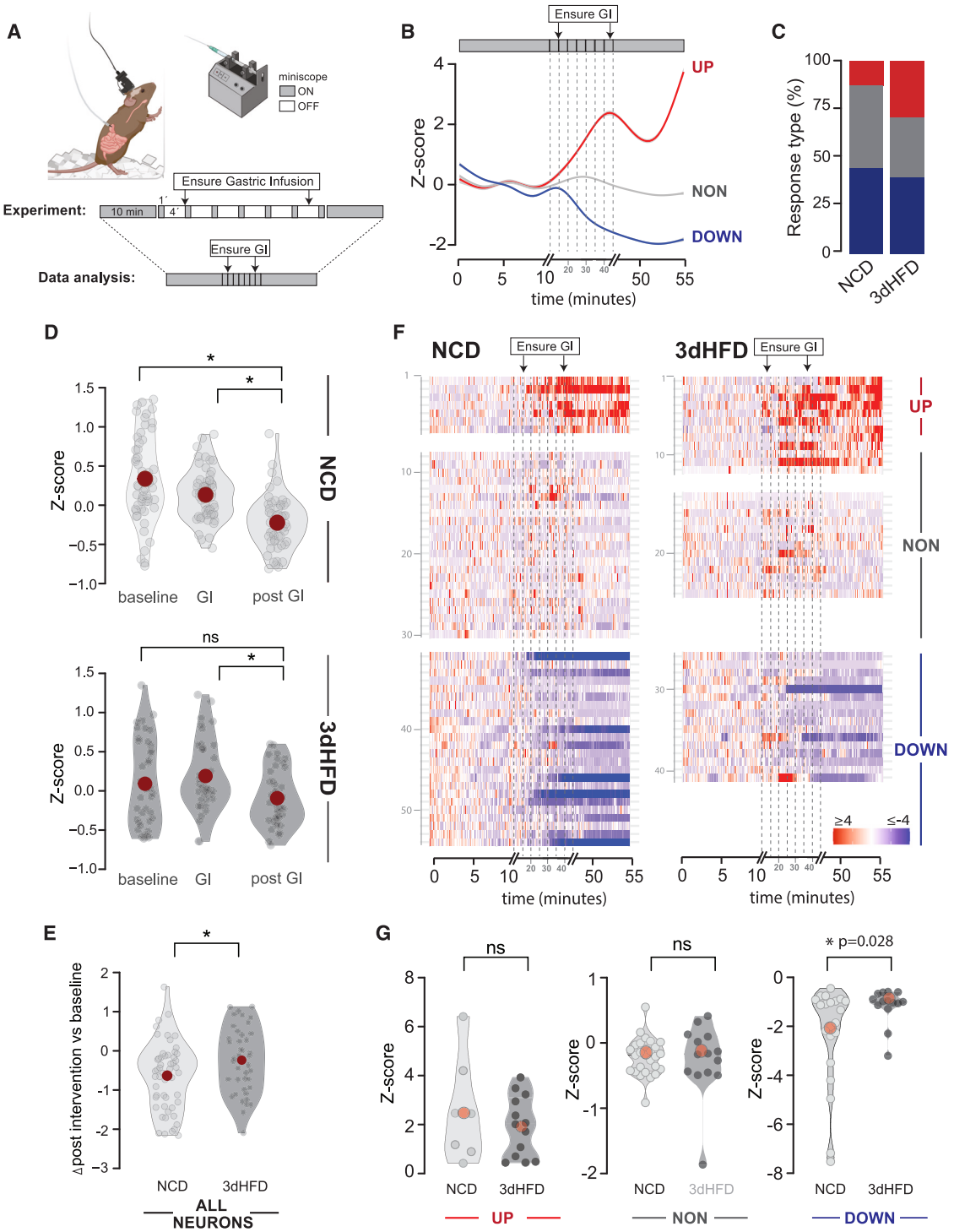

Figure 4. Gastric sensing of nutrients regulates PNOC^{ARC} neuron activity

(A) Experimental setup for simultaneous gastric infusion (GI) and Ca^{2+} imaging. A catheter tubing connects the stomach to the back of the mouse that was fed either NCD or 3dHFD. The recording protocol was 10 min of baseline, 1 min recording every 4 min when infusing (over 31 min), and 10 min postinfusion. Number of mice: 5.

(B) PNOC^{ARC} neuron calcium responses were normalized to their own baseline (*Z* score) and clustered by K-means. Color code: red, activation (UP, 20 neurons); gray, non-responder (NON, 40 neurons); blue, inhibition (DOWN, 35 neurons).

(C) Percentage of neurons per cluster in the context of NCD (108 neurons) or 3dHFD (82 neurons). Red, activation; gray, non-responder; blue, inhibition.

(legend continued on next page)

in PPR (Figure 6H, 0.67 ± 0.16 [NCD] versus 0.62 ± 0.17 [3dHFD]), indicating that alterations in postsynaptic GABA-A receptors mediate the decrease of transmission across the GABAergic BNST → PNOC^{ARC} synapse. To corroborate these findings, we recorded light-evoked currents in the presence of strontium (Sr^{2+}), which favors asynchronous release of neurotransmitter vesicles following ChR2-induced stimulation and provides a direct estimate of postsynaptic efficacy (amplitudes of asynchronous le-IPSCs [asynch-le-IPSCs]) and an indirect assessment of functional synaptic sites (asynch-le-IPSC frequency) in defined circuits.[24] Substitution of Ca^{2+} with Sr^{2+} increases the frequency of asynch-le-IPSCs evoked by light illumination,[24] representing the asynchronous nature of GABA release across the synapse. Analysis of asynch-le-IPSCs recorded in the presence of Sr^{2+} showed that 3dHFD feeding had no effect on the asynch-le-IPSC frequency (Figures 6I and 6J, 11.23 ± 1.2 Hz [NCD] versus 10.43 ± 1.78 Hz [3dHFD]) but decreased the amplitudes of asynch-le-IPSCs (Figures 6I and 6J, 267.7 ± 53.31 pA [NCD] versus 118.6 ± 22.06 pA [3dHFD]). Together, these findings suggest that acute HFD feeding diminishes GABAergic transmission across the BNST → PNOC^{ARC} neuron synapse by causing alterations in postsynaptic GABA-A receptors.

One of the subpopulations present within the BNST are PNOC-expressing neurons. These PNOC^{BNST} neurons were previously reported to modulate feeding behavior by providing inhibitory GABAergic input to AgRP neurons in the ARC.[25] To test whether PNOC^{BNST} neurons are also involved in regulating PNOC^{ARC} activity, we injected an AAV for the Cre-dependent expression of ChR2 (AAV-FLEX-ChR2-mCherry) into the BNST of *PNOC-Cre::PNOC-eGFP* mice and assessed le-IPSCs from GFP-expressing PNOC^{ARC} neurons (Figures 7A and 7B). We observed le-IPSCs in the vast majority of PNOC^{ARC} neurons (Figures 7C and 7D, 82.8% for NCD and 80.7% for 3dHFD). Importantly, 3dHFD feeding evoked a decrease in le-IPSC amplitudes (Figure 7E, 267.7 ± 53.3 pA [NCD] versus 118.6 ± 22.1 pA [3dHFD]) and increased the decay time of le-IPSCs (Figure 7F, 22.44 ± 2.29 ms [NCD] versus 35.51 ± 1.98 ms [3dHFD]), without any apparent changes in PPR (Figure 7G, 0.55 ± 0.07 [NCD] versus 0.53 ± 0.07 [3dHFD]). In addition, recordings of asynch-le-IPSCs in the presence of Sr^{2+} showed that 3dHFD feeding did not alter the frequency (Figure 7I, 4.85 ± 0.88 Hz [NCD] versus 6.18 ± 0.66 [3dHFD]), but decreased the peak amplitudes (Figure 7J, 54.9 ± 5.06 pA [NCD] versus 35.1 ± 4.95 pA [3dHFD]) of asynch-le-IPSCs. In total, these findings demonstrate that PNOC^{BNST} neurons constitute a prominent BNST neuron population that provides GABAergic input to PNOC^{ARC} neurons and that acute HFD feeding evokes postsynaptic alterations of the PNOC^{BNST} → PNOC^{ARC} neuron circuit, diminishing its inhibitory action.

DISCUSSION

PNOC^{ARC} neurons represent a recently identified regulator of food intake during exposure to a highly palatable diet.[16] Here, we show that 3dHFD feeding disinhibits a subcluster of PNOC^{ARC} neurons *in vivo*. When mice are fed an NCD, inhibitory input from PNOC^{BNST} neurons can potently silence PNOC^{ARC} neurons. 3dHFD exposure leads to a reduction in inhibitory transmission from PNOC^{BNST} to PNOC^{ARC} neurons, resulting in a disinhibition of a subset of PNOC^{ARC} neurons, which are readily inhibited by refeeding or intragastric delivery of calories. In turn, the elevated activation of PNOC^{ARC} neurons results in a sizable increase in inhibitory tone to POMC neurons, attenuating satiety by silencing anorexic POMC neurons despite high caloric intake.

PNOC^{ARC} neuron activation accounts for HFD-induced GABAergic inhibition of POMC neurons

3dHFD feeding activates PNOC^{ARC} neurons, which leads to hyperphagia and increases in body weight. We have previously shown that PNOC^{ARC} neurons can provide GABAergic input to POMC neurons and that, in parallel to 3dHFD-induced PNOC^{ARC} neuron activation, inhibitory postsynaptic currents onto POMC neurons increase.[16] These experiments had left open the important question whether and, if so, to what extent PNOC^{ARC} neuron activation accounts for the diet-induced increase in GABAergic inhibition of POMC neurons. This is of particular interest, since it had previously been shown that AgRP neurons can provide inhibitory GABAergic input to POMC neurons.[26] However, chemogenetically inhibiting AgRP neuron activity did not reduce the HFD-induced increase in sIPSCs on POMC neurons,[27] indicating that AgRP neurons do not account for their HFD-induced inhibition. This is consistent with the notion that HFD feeding is still capable of inducing obesity in mice with neonatal ablation of AgRP neurons.[15] In contrast, we reveal that chemogenetic inhibition of PNOC^{ARC} neurons abrogates the HFD-induced increase in GABAergic tone to POMC neurons. Thus, we clearly define PNOC^{ARC} neurons as the functionally relevant source of HFD-induced GABAergic inhibition of POMC neurons.

(D) *Z* score of PNOC^{ARC} neuronal calcium activity before (baseline), during GI, and postintervention (post GI) of mice fed NCD (54 neurons) or 3dHFD (41 neurons). NCD, baseline, 0.33 ± 0.56 *Z* score. NCD, GI, 0.12 ± 0.33 *Z* score. NCD, post GI, −0.24 ± 0.34 *Z* score. 3dHFD, baseline, 0.082 ± 0.55 *Z* score. 3dHFD, GI, 0.18 ± 0.45 *Z* score. 3dHFD, post GI, −0.1 ± 0.36 *Z* score.

(E) Overall degree of suppression in PNOC^{ARC} neurons after GI treatment. *Z* score of PNOC^{ARC} neurons after intervention was compared to their baseline and that of mice fed NCD (54 neurons) or 3dHFD (41 neurons). NCD, 0.57 ± 0.86 *Z* score. 3dHFD, 0.18 ± 0.84 *Z* score.

(F) *Z* score traces of individual PNOC^{ARC} neurons were separated by cluster and diet. *Z* score values 4 ≥ 0 ≤ −4 represent activation > non-responder < inhibition. We limit the maximum *Z* score at 4 for better visualization of the heatmap. NCD: 7 neurons (UP), 26 neurons (NON), 21 neurons (DOWN). 3dHFD: 13 neurons (UP), 14 neurons (NON), 14 neurons (DOWN).

(G) *Z* score post GI of PNOC^{ARC} neurons separated by clusters and diets. UP, NCD, 2.6 ± 2.1 *Z* score. UP, 3dHFD, 3,861.95 ± 1.2 *Z* score. NON, NCD, −0.22 ± 0.28 *Z* score. NON, 3dHFD, −0.25 ± 0.54 *Z* score. DOWN, NCD, −2.3 ± 2 *Z* score. DOWN, 3dHFD, −1.2 ± 0.71 *Z* score. NCD: 7 neurons (UP), 26 neurons (NON), 21 neurons (DOWN). 3dHFD: 13 neurons (UP), 14 neurons (NON), 14 neurons (DOWN). Statistical analysis was performed using Fisher's exact test (C), Games-Howell test (D), Welch's t test (E), and one-tailed t test (G). ns, not significant; *$p \leq 0.05$.

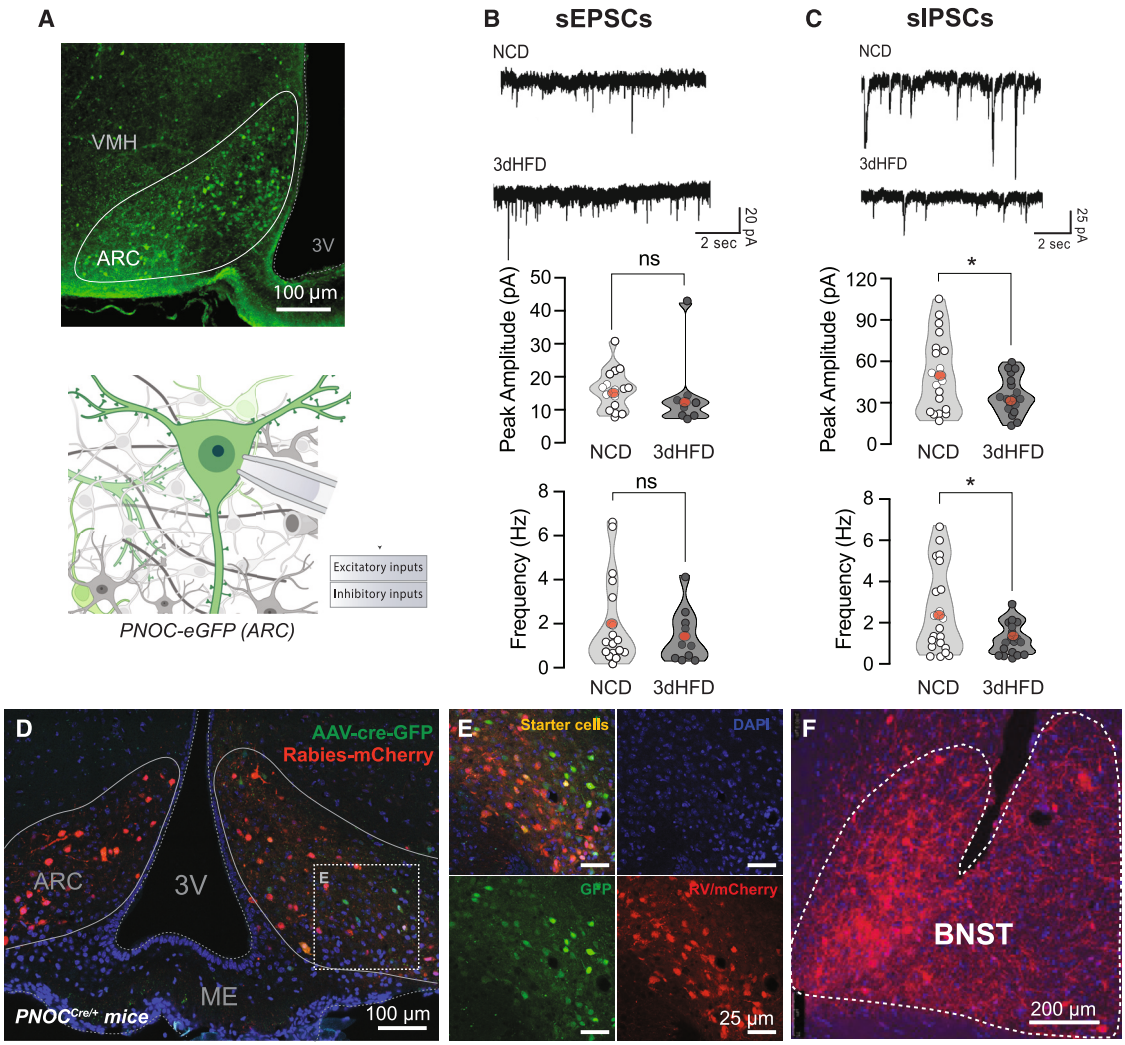

Figure 5. 3dHFD feeding attenuates inhibitory inputs to PNOC^{ARC} neurons

(A) Acute brain slices of *PNOC-eGFP* mice after NCD or 3dHFD were used to record spontaneous synaptic inputs to PNOC^{ARC} neurons (scale bar, 100 μm).

(B) Spontaneous excitatory postsynaptic currents (sEPSCs). Top: representative traces of sEPSCs on PNOC^{ARC} neurons after NCD (top) and 3dHFD (bottom). sEPSC peak amplitude (middle) and frequency (bottom) of PNOC^{ARC} neurons after NCD or 3dHFD. Peak amplitude, NCD, 16.13 ± 1.5 pA. Peak amplitude, 3dHFD, 13.7 ± 3.3 pA. Frequency, NCD, 2.06 ± 0.51 Hz. Frequency, 3dHFD, 1.45 ± 0.39 Hz. Number of mice: 3 (NCD) and 3 (3dHFD). Number of cells: 17 (NCD) and 10 (3dHFD).

(C) Spontaneous inhibitory postsynaptic currents (sIPSCs). Top: representative traces of sIPSCs on PNOC^{ARC} neurons after NCD (top) and 3dHFD (bottom). sIPSC peak amplitude (middle) and frequency (bottom) of PNOC^{ARC} neurons after NCD or 3dHFD. Peak amplitude, NCD, 50.8 ± 6.4 pA. Peak amplitude, 3dHFD, 35.2 ± 3.3 pA. Frequency, NCD, 2.71 ± 0.48 Hz. Frequency, 3dHFD, 1.3 ± 0.18 Hz. Number of mice: 3 (NCD) and 3 (3dHFD). Number of cells: 19 (NCD) and 18 (3dHFD).

(D) Example image of ARC injection site. eGFP labels PNOC^{ARC} neurons (green) and mCherry detects rabies-infected monosynaptic upstream inputs (red) (blue, DAPI; scale bar, 100 μm).

(E) Characterization of the distribution pattern of starter neurons (green) and retrogradely labeled neurons (red) in the ARC (scale bars, 25 μm).

(F) Representative image of rabies-labeled neurons in the BNST (scale bar, 200 μm). Statistical analysis was performed using unpaired two-tailed Student's t tests (B and C). ns, not significant; *$p \leq 0.05$.

Given that PNOC neurons release not only GABA but also nociceptin, we further investigated the potential role of nociceptin release from these cells during 3dHFD-induced POMC cell inhibition and PNOC^{ARC} neuron activation-dependent hyperphagia. We found that even low concentrations of nociceptin can, upon pharmacological application, silence POMC neurons *ex vivo* by inducing outward currents consistent with previous electrophysiological studies.[28,29] Previous research has demonstrated that injection of nociceptin and nociceptin receptor agonists into the cerebrospinal fluid induces hyperphagia.[30–34] However, *in vivo*, lack of nociceptin release does not abrogate the ability of PNOC^{ARC} neuron activation to promote hyperphagia. Taking these results together, nociceptin has the ability to silence POMC neurons *in situ*; however, it likely does not contribute to

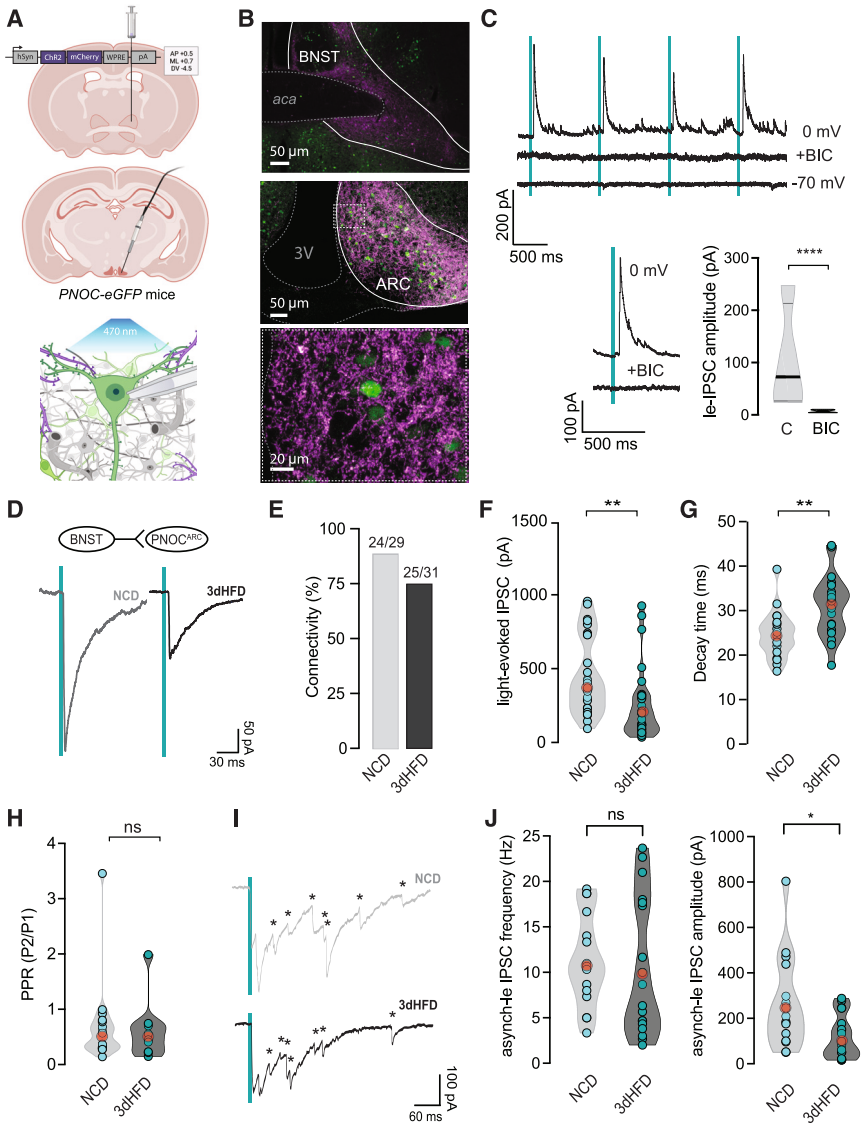

Figure 6. 3dHFD feeding diminishes transmission across the GABAergic BNST → PNOC^{ARC} neuron synapse

(A) Schematic of experimental approach. AAVhSyn-ChR2-mCherry was injected into the BNST of *PNOC-eGFP* mice.

(B) Example images showing ChR2-mCherry expression (magenta) in the BNST and ARC of *PNOC-eGFP* (green) mice. Scale bars, 50 μm for BNST and ARC, 20 μm for ARC zoom (bottom).

(C) Top: example traces of light-evoked (blue vertical bar) postsynaptic currents (le-IPSCs) recorded from PNOC^{ARC} neurons. le-IPSCs were observed at V_h = 0 mV (top) and were blocked by application of bicuculline (BIC). We did not detect le-EPSCs at V_h = −70 mV holding potential. Bottom: quantification of le-IPSC amplitude in control (C) and BIC recording conditions (104.10 ± 51.43 pA [control] versus 7.05 ± 1.58 pA [BIC]). Number of mice: 2. Number of cells: 4 (control) and 4 (BIC).

(D–J) We examined connectivity strength by assessing connectivity, le (light-evoked)-IPSC amplitude, PPR (paired pulse ratio), and asynchronous release properties in NCD- or 3dHFD-fed mice. (D) Representative example traces of le-IPSCs recorded at V_h = −70 mV (high chloride-containing internal solution; see STAR Methods) from brain slices of control (NCD) and 3dHFD mice (light stimulus indicated by blue vertical bar). (E) Connectivity ratio of BNST → PNOC^{ARC} neurons. (F) le-IPSC amplitude (452 ± 49 pA [NCD] versus 251 ± 43 pA [3dHFD]). (G) Decay time of le-IPSCs in NCD- or 3dHFD-fed mice (24.6 ± 1.12 ms [NCD] versus 31 ± 1.5 ms [3dHFD]). (H) Paired pulse ratio in NCD- or 3dHFD-fed mice (0.67 ± 0.16 [NCD] versus 0.62 ± 0.17 [3dHFD]). Number of mice: 3 (NCD) and 4 (3dHFD). Number of cells: 29 (NCD) and 31 (3dHFD). (I) Example traces of le-IPSCs of PNOC^{BNST} → PNOC^{ARC} with Sr^{2+}-artificial cerebrospinal fluid (aCSF) of NCD-fed (top) or 3dHFD-fed (bottom) mice. Light stimulus is indicated by the blue vertical bar. (J) Asynchronous (asynch) frequency (left) and peak amplitude (right) analysis of le-IPSCs in Sr^{+} recording conditions from NCD- or 3dHFD-fed mice. Frequency: 11.23 ± 1.2 Hz (NCD) versus 10.43 ± 1.78 Hz (3dHFD). Amplitude: 267.7 ± 53.3 pA (NCD) versus 118.6 ± 22 pA (3dHFD). Number of mice: 3 (NCD) and 3 (3dHFD). Number of cells: 15 (NCD) and 18 (3dHFD). Statistical analysis was performed using unpaired two-tailed Student's t tests (F–H and J). ns, not significant; $^{**}p \leq 0.01$.

acute HFD-induced hyperphagia caused by activation of PNOC^{ARC} neurons *in vivo*.

PNOC^{ARC} neurons are molecularly and functionally heterogeneous

Using single-cell Ca^{2+} imaging in freely behaving mice, we show that PNOC^{ARC} neurons represent a largely heterogeneous population, whose activity profiles are distinct from more homogenously regulated AgRP and POMC neurons. In accordance with the observed heterogeneous activity profiles, single-cell sequencing of PNOC^{ARC} neurons revealed that the entire PNOC^{ARC} population consists of several molecularly distinct subpopulations.[17] PNOC^{ARC} neuron molecular heterogeneity can be subdivided into two major cluster families: somatostatin (*Sst*) and cellular retinoic acid binding protein 1 (*Crabp1*) PNOC-positive cells. Notably, other ARC populations respond much more uniformly to dietary stimuli. The majority of POMC neurons are activated, while AgRP neurons are inhibited by presentation and ingestion of food.[11] Thus, future work will clearly have to delineate the specific function of heterogeneous, molecularly distinct PNOC^{ARC} cell clusters.

PNOC^{ARC} neurons are mainly regulated through postingestive stimuli

PNOC^{ARC} neuron activity appears to be mainly controlled by nutrient sensing, as GI of Ensure more strongly inhibited PNOC^{ARC} neurons than the immediate response observed upon food presentation. We postulate that the inflow of nutrients can be transmitted through vagal afferents that innervate the stomach and intestinal system. In turn, these vagal afferents

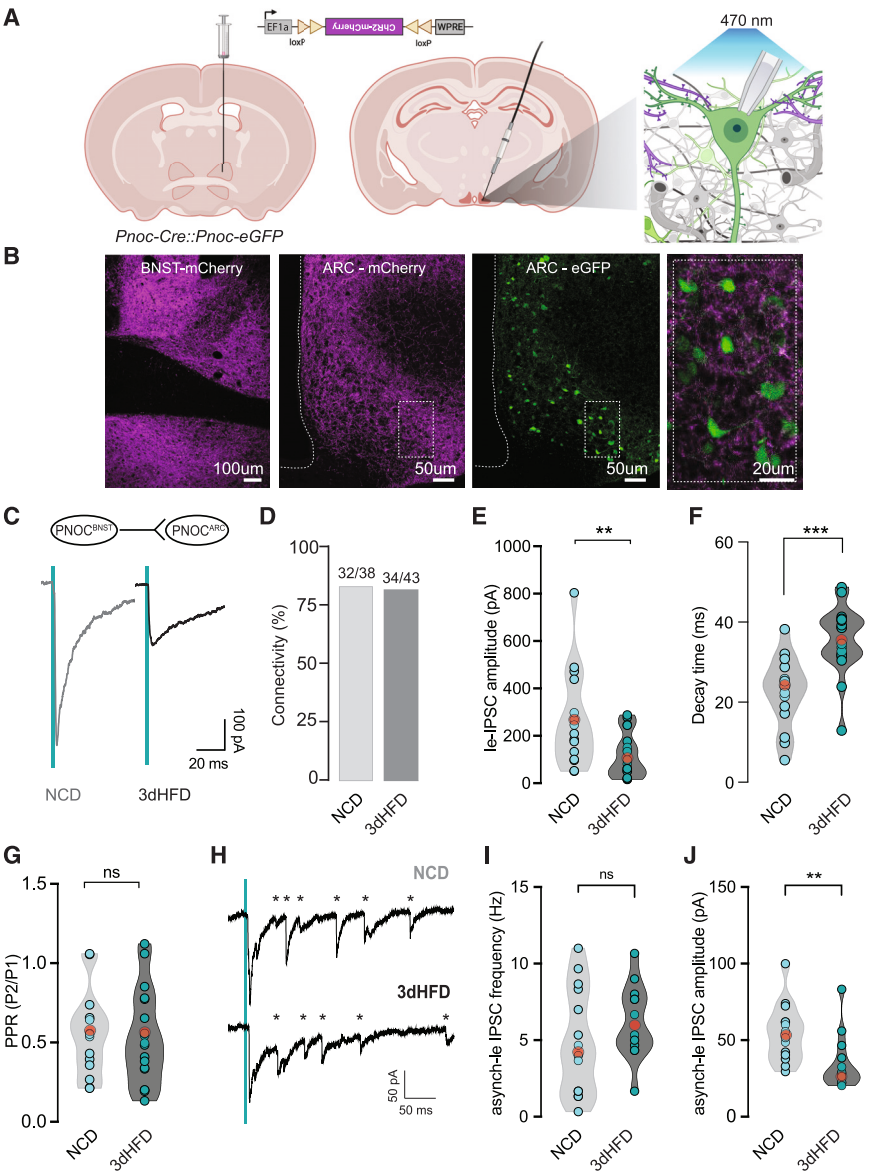

Figure 7. Disinhibition of PNOC^{BNST} → PNOC^{ARC} circuitry after 3dHFD

(A) To study PNOC^{BNST} regulation of PNOC^{ARC} neuron activity, hSyn-FLEX-ChR2-mCherry was injected into the BNST of *PNOC-Cre::PNOC-eGFP* mice, and *PNOC-eGFP* neurons from the ARC were recorded.

(B) Example images of ChR2-mCherry expression in the BNST and innervation of the ARC (eGFP in green, ChR2-mCherry in magenta) (scale bars, 100 μm (BNST, left), 50 μm (ARC, middle), and 20 μm (ARC higher resolution, right).

(C–G) We examined connectivity strength by assessing connectivity, Ie (light-evoked)-IPSC amplitude, and PPR (paired pulse ratio) in NCD- or 3dHFD-fed mice (light stimulus indicated by blue vertical bar). (C) Example traces of Ie-IPSCs from PNOC^{BNST} → PNOC^{ARC} neurons. (D) Connectivity ratio of PNOC^{BNST} → PNOC^{ARC} neurons. (E) Ie-IPSC amplitude (268 ± 53 pA [NCD] versus 119 ± 22 pA [3dHFD]). (F) Decay time of Ie-IPSCs in NCD- or 3dHFD-fed mice (22.4 ± 2.3 ms [NCD] versus 35.5 ± 2 ms [3dHFD]). (G) Paired pulse ratio in NCD- or 3dHFD-fed mice (0.55 ± 0.07 [NCD] versus 0.53 ± 0.07 [3dHFD]). Number of mice: 3 (NCD) and 3 (3dHFD). Number of cells: 18 (NCD) and 15 (3dHFD).

(H) Ie-IPSCs of PNOC^{BNST} → PNOC^{ARC} with Sr^{+}-aCSF of NCD-fed mice or 3dHFD-fed mice (light stimulus indicated by blue vertical bar).

(I and J) Asynchronous (asynch) frequency (I) and peak amplitude (J) analysis of Ie-IPSCs in Sr^{2+} recording conditions from NCD- or 3dHFD-fed mice. A period of 300 ms was analyzed 25 ms after the light pulse. Frequency: 4.85 ± 0.88 Hz (NCD) versus 6.18 ± 0.66 Hz (3dHFD). Amplitude: 54.9 ± 5 pA (NCD) versus 35.1 ± 5 pA (3dHFD). Number of mice: 3 (NCD) and 3 (3dHFD). Number of cells: 14 (NCD) and 13 (3dHFD). Statistical analysis was performed using unpaired two-tailed Student's t tests (E–G, I, and J). ns, not significant; $^{**}p \leq 0.01$, $^{***}p \leq 0.001$.

transfer information regarding the nutrient content to neurons of the nucleus tractus solitarius (NTS) and can, through a wide variety of projection patterns, influence the activity profile of PNOC^{ARC} neurons. As PNOC^{ARC} activation profiles were altered upon GI of nutrients, input from the gut-brain axis appears to an important regulatory mechanism of PNOC^{ARC} neurons.

Disinhibition of PNOC^{ARC} neurons after 3dHFD feeding

3dHFD reduces the degree of inhibition of the inhibited subcluster of PNOC^{ARC} neurons to both refeeding and GI. We hypothesized that acute 3dHFD feeding could increase PNOC^{ARC} activity through cell intrinsic changes and/or through plasticity in its presynaptic inputs. Using electrophysiology, we demonstrate that PNOC^{ARC} neurons are disinhibited upon 3dHFD feeding, a finding that provides a mechanistic explanation for the attenuated inhibition observed in a subpopulation of PNOC^{ARC} neurons. Hence, disinhibition appears to play a crucial role in the increased activation of PNOC^{ARC} neurons under acute 3dHFD feeding.

PNOC^{BNST} → PNOC^{ARC} disinhibition enables PNOC^{ARC} activation upon 3dHFD feeding

The BNST is a limbic structure that is an integration site for primary behavioral responses such as stress, fear, reward, memory, and feeding. Interestingly, *Pnoc* expression levels within the BNST are very high.[35–37] PNOC^{BNST} neurons are known to inhibit neuronal populations in the ARC, such as the AgRP neurons, through GABA release.[25] PNOC^{BNST} neuronal stimulation prevents mice from eating, while ablation of PNOC^{BNST} neurons causes obesity due to increases in food intake, resulting in expansion of white fat tissue mass.[25,38–40] Our findings demonstrate that PNOC^{BNST} neurons also project to and inhibit

PNOC^{ARC} neurons. Furthermore, this inhibition is reduced after 3dHFD feeding. With a similar excitatory, but reduced inhibitory, tone, PNOC^{ARC} neurons can increase their activity levels. Further experiments will have to delineate the mechanisms of how post-ingestive calorie sensing modulates activity of PNOC^{BNST} neurons. Nevertheless, our experiments reveal an interesting regulatory pathway, where altered activity of a neurocircuitry from the BNST leads to activation of PNOC^{ARC} neurons to mediate GABAergic inhibition of POMC neurons upon consumption of highly palatable food. Therefore, reinstating proper inhibition of PNOC^{ARC} neurons may provide a promising avenue for preventing or treating obesity resulting from overconsumption of highly palatable, calorie-dense food.

Limitations of the study

PNOC^{ARC} neurons modulate downstream neurons through the release of inhibitory neurotransmitters such as GABA, nociceptin, and potentially other neuropeptides. Our results demonstrate that the acute HFD-induced hyperphagia phenotype instigated by activation of PNOC^{ARC} neurons does not require nociceptin release and is paired with changes in GABAergic tone to POMC neurons. We used an optogenetic stimulation paradigm (20 Hz, 5 ms pulse, 1 s ON-3 s OFF), previously published by Jais et al.,[16] optimizing reliable GABA release without inducing thermal damage to the brain or stimulating food intake in control mice lacking ChR2 expression in PNOC neurons. However, such a stimulation sequence is suboptimal to induce peptide release, as it only stimulated for 1 of 4 s and employed the standard ChR2 variant, with kinetics that are likely insufficiently fast to induce peptide release. To conclusively prove the GABAergic nature of PNOC^{ARC}-induced hyperphagia, we attempted to generate PNOC VGAT KO mice, but failed due to continuous germline deletion. Hence, we cannot rule out any additional roles of neuropeptide release from PNOC^{ARC} neurons in orchestrating acute HFD-induced hyperphagia. Finally, most results represent pooled data from male and female mice, thus limiting the interpretation with respect to potential sexually dimorphic phenotypes.

STAR★METHODS

Detailed methods are provided in the online version of this paper and include the following:

SUPPLEMENTAL INFORMATION

Supplemental information can be found online at https://doi.org/10.1016/j.celrep.2024.114343.

ACKNOWLEDGMENTS

We thank Christian Heilinger, Pia Scholl, Nadine Zgoda, Christiane Schäfer, and Andreas Beyrau for excellent technical assistance. Ursula Lichtenberg, Hella Brönneke, and Karina Schöfisch always provided skillful administrative help. We appreciate the scientific counsel from Weiyi Chen, Lukas Steuernagel, and Marie Holm Solheim. This work was funded in part by Novo Nordisk (to J.C.B. and H.F.), the Center for Molecular Medicine Cologne (CMMC) (to J.C.B.), the German National Diabetes Center (DZD) (to J.C.B.), and the European Research Council (SYNEME 742106 to J.C.B. and GuMeCo 851778 to H.F.); funding from the Deutsche Forschungsgemeinschaft (DFG, German Research Foundation; grant ID 409551513); a Forum grant of the UoC Excellent Research Support Program (to P. Kloppenburg); and the Lundbeck Foundation (to D.B.).

AUTHOR CONTRIBUTIONS

J.C.B., H.F., T.S.-H., and M.M. conceived the study. T.S.-H. and M.M. wrote the original draft of the manuscript. All coauthors reviewed and edited the manuscript. T.S.-H. and M.M. performed surgeries for electrophysiological circuit mapping. M.M. performed all circuit mapping and spontaneous input electrophysiological recordings and analyses. T.S.-H. performed all other surgeries. D.B. performed gastric catheter cannulations. T.S.-H. carried out all Inscopix analyses and postmortem validation. D.W.-L. contributed to the Inscopix analysis pipeline. P. Klemm performed clustering of neurons and statistical analysis. S.C. measured the nociceptin effect on POMC neurons. A.J. and T.S.-H. performed optogenetics and PhenoMaster experiments. X.J., D.B., and T.S.-H. analyzed input areas of rabies tracing. T.S.-H. performed *in situ* hybridization and analysis. J.C.B., H.F., and P. Kloppenburg provided resources.

DECLARATION OF INTERESTS

J.C.B. is a cofounder of Cerapeutix and has received research funding through collaborations with Sanofi Aventis and Novo Nordisk, Inc. He also consulted for Eli Lilly and Company and Novo Nordisk, all of which did not affect the content of this article.

Received: October 10, 2023
Revised: March 1, 2024
Accepted: May 23, 2024
Published: June 11, 2024

REFERENCES

1. Drewnowski, A. (2007). The real contribution of added sugars and fats to obesity. Epidemiol. Rev. *29*, 160–171. https://doi.org/10.1093/epirev/mxm011.
2. Jais, A., and Brüning, J.C. (2022). Arcuate Nucleus-Dependent Regulation of Metabolism-Pathways to Obesity and Diabetes Mellitus. Endocr. Rev. *43*, 314–328. https://doi.org/10.1210/endrev/bnab025.
3. Andermann, M.L., and Lowell, B.B. (2017). Toward a Wiring Diagram Understanding of Appetite Control. Neuron *95*, 757–778. https://doi.org/10.1016/j.neuron.2017.06.014.
4. Tong, Q., Ye, C.P., Jones, J.E., Elmquist, J.K., and Lowell, B.B. (2008). Synaptic release of GABA by AgRP neurons is required for normal regulation of energy balance. Nat. Neurosci. *11*, 998–1000. https://doi.org/10.1038/nn.2167.

5. Hahn, T.M., Breininger, J.F., Baskin, D.G., and Schwartz, M.W. (1998). Coexpression of Agrp and NPY in fasting-activated hypothalamic neurons. Nat. Neurosci. *1*, 271–272. https://doi.org/10.1038/1082.

6. Krashes, M.J., Shah, B.P., Koda, S., and Lowell, B.B. (2013). Rapid versus delayed stimulation of feeding by the endogenously released AgRP neuron mediators GABA, NPY, and AgRP. Cell Metabol. *18*, 588–595. https://doi.org/10.1016/j.cmet.2013.09.009.

7. Fenselau, H., Campbell, J.N., Verstegen, A.M.J., Madara, J.C., Xu, J., Shah, B.P., Resch, J.M., Yang, Z., Mandelblat-Cerf, Y., Livneh, Y., and Lowell, B.B. (2017). A rapidly acting glutamatergic ARC→PVH satiety circuit postsynaptically regulated by alpha-MSH. Nat. Neurosci. *20*, 42–51. https://doi.org/10.1038/nn.4442.

8. D'Agostino, G., and Diano, S. (2010). Alpha-melanocyte stimulating hormone: production and degradation. J. Mol. Med. *88*, 1195–1201. https://doi.org/10.1007/s00109-010-0651-0.

9. Garfield, A.S., Li, C., Madara, J.C., Shah, B.P., Webber, E., Steger, J.S., Campbell, J.N., Gavrilova, O., Lee, C.E., Olson, D.P., et al. (2015). A neural basis for melanocortin-4 receptor-regulated appetite. Nat. Neurosci. *18*, 863–871. https://doi.org/10.1038/nn.4011.

10. Betley, J.N., and Sternson, S.M. (2015). Applying the Brakes: When to Stop Eating. Neuron *88*, 440–441. https://doi.org/10.1016/j.neuron.2015.10.034.

11. Chen, Y., Lin, Y.C., Kuo, T.W., and Knight, Z.A. (2015). Sensory detection of food rapidly modulates arcuate feeding circuits. Cell *160*, 829–841. https://doi.org/10.1016/j.cell.2015.01.033.

12. Mandelblat-Cerf, Y., Ramesh, R.N., Burgess, C.R., Patella, P., Yang, Z., Lowell, B.B., and Andermann, M.L. (2015). Arcuate hypothalamic AgRP and putative POMC neurons show opposite changes in spiking across multiple timescales. Elife *4*, e07122. https://doi.org/10.7554/eLife.07122.

13. Brandt, C., Nolte, H., Henschke, S., Engström Ruud, L., Awazawa, M., Morgan, D.A., Gabel, P., Sprenger, H.G., Hess, M.E., Günther, S., et al. (2018). Food Perception Primes Hepatic ER Homeostasis via Melanocortin-Dependent Control of mTOR Activation. Cell *175*, 1321–1335.e20. https://doi.org/10.1016/j.cell.2018.10.015.

14. Henschke, S., Nolte, H., Magoley, J., Kleele, T., Brandt, C., Hausen, A.C., Wunderlich, C.M., Bauder, C.A., Aschauer, P., Manley, S., et al. (2024). Food perception promotes phosphorylation of MFFS131 and mitochondrial fragmentation in liver. Science *384*, 438–446. https://doi.org/10.1126/science.adk1005.

15. Denis, R.G.P., Joly-Amado, A., Webber, E., Langlet, F., Schaeffer, M., Padilla, S.L., Cansell, C., Dehouck, B., Castel, J., Delbès, A.S., et al. (2015). Palatability Can Drive Feeding Independent of AgRP Neurons. Cell Metabol. *22*, 646–657. https://doi.org/10.1016/j.cmet.2015.07.011.

16. Jais, A., Paeger, L., Sotelo-Hitschfeld, T., Bremser, S., Prinzensteiner, M., Klemm, P., Mykytiuk, V., Widdershooven, P.J.M., Vesting, A.J., Grzelka, K., et al. (2020). PNOC(ARC) Neurons Promote Hyperphagia and Obesity upon High-Fat-Diet Feeding. Neuron *106*, 1009–1025.e10. https://doi.org/10.1016/j.neuron.2020.03.022.

17. Steuernagel, L., Lam, B.Y.H., Klemm, P., Dowsett, G.K.C., Bauder, C.A., Tadross, J.A., Hitschfeld, T.S., Del Rio Martin, A., Chen, W., de Solis, A.J., et al. (2022). HypoMap—a unified single-cell gene expression atlas of the murine hypothalamus. Nat. Metab. *4*, 1402–1419. https://doi.org/10.1038/s42255-022-00657-y.

18. Chee, M.J., Price, C.J., Statnick, M.A., and Colmers, W.F. (2011). Nociceptin/orphanin FQ suppresses the excitability of neurons in the ventromedial nucleus of the hypothalamus. J. Physiol. *589*, 3103–3114. https://doi.org/10.1113/jphysiol.2011.208819.

19. Wang, D., He, X., Zhao, Z., Feng, Q., Lin, R., Sun, Y., Ding, T., Xu, F., Luo, M., and Zhan, C. (2015). Whole-brain mapping of the direct inputs and axonal projections of POMC and AgRP neurons. Front. Neuroanat. *9*, 40. https://doi.org/10.3389/fnana.2015.00040.

20. Kudo, T., Uchigashima, M., Miyazaki, T., Konno, K., Yamasaki, M., Yanagawa, Y., Minami, M., and Watanabe, M. (2012). Three types of neurochemical projection from the bed nucleus of the stria terminalis to the ventral tegmental area in adult mice. J. Neurosci. *32*, 18035–18046. https://doi.org/10.1523/JNEUROSCI.4057-12.2012.

21. Resch, J.M., Fenselau, H., Madara, J.C., Wu, C., Campbell, J.N., Lyubetskaya, A., Dawes, B.A., Tsai, L.T., Li, M.M., Livneh, Y., et al. (2017). Aldosterone-Sensing Neurons in the NTS Exhibit State-Dependent Pacemaker Activity and Drive Sodium Appetite via Synergy with Angiotensin II Signaling. Neuron *96*, 190–206.e7. https://doi.org/10.1016/j.neuron.2017.09.014.

22. Crestani, C.C., Alves, F.H., Gomes, F.V., Resstel, L.B., Correa, F.M., and Herman, J.P. (2013). Mechanisms in the bed nucleus of the stria terminalis involved in control of autonomic and neuroendocrine functions: a review. Curr. Neuropharmacol. *11*, 141–159. https://doi.org/10.2174/1570159X11311020002.

23. Hammack, S.E., Braas, K.M., and May, V. (2021). Chemoarchitecture of the bed nucleus of the stria terminalis: Neurophenotypic diversity and function. Handb. Clin. Neurol. *179*, 385–402. https://doi.org/10.1016/B978-0-12-819975-6.00025-X.

24. Grzelka, K., Wilhelms, H., Dodt, S., Dreisow, M.L., Madara, J.C., Walker, S.J., Wu, C., Wang, D., Lowell, B.B., and Fenselau, H. (2023). A synaptic amplifier of hunger for regaining body weight in the hypothalamus. Cell Metabol. *35*, 770–785.e5. https://doi.org/10.1016/j.cmet.2023.03.002.

25. Smith, M.A., Choudhury, A.I., Glegola, J.A., Viskaitis, P., Irvine, E.E., de Campos Silva, P.C.C., Khadayate, S., Zeilhofer, H.U., and Withers, D.J. (2020). Extrahypothalamic GABAergic nociceptin-expressing neurons regulate AgRP neuron activity to control feeding behavior. J. Clin. Invest. *130*, 126–142. https://doi.org/10.1172/JCI130340.

26. Cowley, M.A., Smart, J.L., Rubinstein, M., Cerdán, M.G., Diano, S., Horvath, T.L., Cone, R.D., and Low, M.J. (2001). Leptin activates anorexigenic POMC neurons through a neural network in the arcuate nucleus. Nature *411*, 480–484. https://doi.org/10.1038/35078085.

27. Rau, A.R., and Hentges, S.T. (2017). The Relevance of AgRP Neuron-Derived GABA Inputs to POMC Neurons Differs for Spontaneous and Evoked Release. J. Neurosci. *37*, 7362–7372. https://doi.org/10.1523/JNEUROSCI.0647-17.2017.

28. Sayers, S., Le, N., Hernandez, J., Mata-Pacheco, V., and Wagner, E.J. (2022). The vital role of arcuate nociceptin/orphanin FQ neurones in mounting an oestradiol-dependent adaptive response to negative energy balance via inhibition of nearby proopiomelanocortin neurones. J. Physiol. *600*, 4939–4961. https://doi.org/10.1113/JP283378.

29. Hernandez, J., Fabelo, C., Perez, L., Moore, C., Chang, R., and Wagner, E.J. (2019). Nociceptin/orphanin FQ modulates energy homeostasis through inhibition of neurotransmission at VMN SF-1/ARC POMC synapses in a sex- and diet-dependent manner. Biol. Sex Differ. *10*, 9. https://doi.org/10.1186/s13293-019-0220-3.

30. Ciccocioppo, R., Biondini, M., Antonelli, L., Wichmann, J., Jenck, F., and Massi, M. (2002). Reversal of stress- and CRF-induced anorexia in rats by the synthetic nociceptin/orphanin FQ receptor agonist, Ro 64-6198. Psychopharmacology (Berl) *161*, 113–119. https://doi.org/10.1007/s00213-002-1020-7.

31. Leventhal, L., Mathis, J.P., Rossi, G.C., Pasternak, G.W., and Bodnar, R.J. (1998). Orphan opioid receptor antisense probes block orphanin FQ-induced hyperphagia. Eur. J. Pharmacol. *349*, R1–R3. https://doi.org/10.1016/s0014-2999(98)00272-6.

32. Matsushita, H., Ishihara, A., Mashiko, S., Tanaka, T., Kanno, T., Iwaasa, H., Ohta, H., and Kanatani, A. (2009). Chronic intracerebroventricular infusion of nociceptin/orphanin FQ produces body weight gain by affecting both feeding and energy metabolism in mice. Endocrinology *150*, 2668–2673. https://doi.org/10.1210/en.2008-1515.

33. Pomonis, J.D., Billington, C.J., and Levine, A.S. (1996). Orphanin FQ, agonist of orphan opioid receptor ORL1, stimulates feeding in rats. Neuroreport *8*, 369–371. https://doi.org/10.1097/00001756-199612200-00072.

34. Polidori, C., de Caro, G., and Massi, M. (2000). The hyperphagic effect of nociceptin/orphanin FQ in rats. Peptides *21*, 1051–1062. https://doi.org/10.1016/s0196-9781(00)00243-6.

35. Ikeda, K., Watanabe, M., Ichikawa, T., Kobayashi, T., Yano, R., and Kumanishi, T. (1998). Distribution of prepro-nociceptin/orphanin FQ mRNA and its receptor mRNA in developing and adult mouse central nervous systems. J. Comp. Neurol. *399*, 139–151. https://doi.org/10.1002/(sici)1096-9861(19980914)399:1<139::aid-cne11>3.0.co;2-c.

36. Boom, A., Mollereau, C., Meunier, J.C., Vassart, G., Parmentier, M., Vanderhaeghen, J.J., and Schiffmann, S.N. (1999). Distribution of the nociceptin and nocistatin precursor transcript in the mouse central nervous system. Neuroscience *91*, 991–1007. https://doi.org/10.1016/s0306-4522(98)00683-6.

37. Parker, K.E., Pedersen, C.E., Gomez, A.M., Spangler, S.M., Walicki, M.C., Feng, S.Y., Stewart, S.L., Otis, J.M., Al-Hasani, R., McCall, J.G., et al. (2019). A Paranigral VTA Nociceptin Circuit that Constrains Motivation for Reward. Cell *178*, 653–671.e19. https://doi.org/10.1016/j.cell.2019.06.034.

38. Ung, R.L., Ortiz-Juza, M.M., Curtis, V.R., Alghorazi, R.A., Velazquez-Hernandez, G., Ring, A., Garcia-Reyes, R.A., Stuber, G.D., Zhou, P., Kato, H.K., et al. (2022). Prepronociceptin-expressing neurons in the extended amygdala signal darting away from an aversive odor. Preprint at bioRxiv. https://doi.org/10.1101/2022.02.21.481217.

39. Rodriguez-Romaguera, J., Ung, R.L., Nomura, H., Otis, J.M., Basiri, M.L., Namboodiri, V.M.K., Zhu, X., Robinson, J.E., van den Munkhof, H.E., McHenry, J.A., et al. (2020). Prepronociceptin-Expressing Neurons in the Extended Amygdala Encode and Promote Rapid Arousal Responses to Motivationally Salient Stimuli. Cell Rep. *33*, 108362. https://doi.org/10.1016/j.celrep.2020.108362.

40. Hardaway, J.A., Halladay, L.R., Mazzone, C.M., Pati, D., Bloodgood, D.W., Kim, M., Jensen, J., DiBerto, J.F., Boyt, K.M., Shiddapur, A., et al. (2019). Central Amygdala Prepronociceptin-Expressing Neurons Mediate Palatable Food Consumption and Reward. Neuron *102*, 1037. https://doi.org/10.1016/j.neuron.2019.03.037.

41. Krashes, M.J., Koda, S., Ye, C., Rogan, S.C., Adams, A.C., Cusher, D.S., Maratos-Flier, E., Roth, B.L., and Lowell, B.B. (2011). Rapid, reversible activation of AgRP neurons drives feeding behavior in mice. J. Clin. Invest. *121*, 1424–1428. https://doi.org/10.1172/JCI46229.

42. Chen, T.W., Wardill, T.J., Sun, Y., Pulver, S.R., Renninger, S.L., Baohan, A., Schreiter, E.R., Kerr, R.A., Orger, M.B., Jayaraman, V., et al. (2013). Ultrasensitive fluorescent proteins for imaging neuronal activity. Nature *499*, 295–300. https://doi.org/10.1038/nature12354.

43. Schindelin, J., Arganda-Carreras, I., Frise, E., Kaynig, V., Longair, M., Pietzsch, T., Preibisch, S., Rueden, C., Saalfeld, S., Schmid, B., et al. (2012). Fiji: an open-source platform for biological-image analysis. Nat. Methods *9*, 676–682. https://doi.org/10.1038/nmeth.2019.

44. Giovannucci, A., Friedrich, J., Gunn, P., Kalfon, J., Brown, B.L., Koay, S.A., Taxidis, J., Najafi, F., Gauthier, J.L., Zhou, P., et al. (2019). CaImAn an open source tool for scalable calcium imaging data analysis. eLife *8*, e38173. https://doi.org/10.7554/eLife.38173.

45. Ueno, S., Yoshida, S., Mondal, A., Nishina, K., Koyama, M., Sakata, I., Miura, K., Hayashi, Y., Nemoto, N., Nishigaki, K., and Sakai, T. (2012). In vitro selection of a peptide antagonist of growth hormone secretagogue receptor using cDNA display. Proc. Natl. Acad. Sci. USA *109*, 11121–11126. https://doi.org/10.1073/pnas.1203561109.

46. Ye, J.H., Zhang, J., Xiao, C., and Kong, J.Q. (2006). Patch-clamp studies in the CNS illustrate a simple new method for obtaining viable neurons in rat brain slices: glycerol replacement of NaCl protects CNS neurons. J. Neurosci. Methods *158*, 251–259. https://doi.org/10.1016/j.jneumeth.2006.06.006.

47. Hess, S., Wratil, H., and Kloppenburg, P. (2023). Perforated Patch Clamp Recordings in ex vivo Brain Slices from Adult Mice. Bio. Protoc. *13*, e4741. https://doi.org/10.21769/BioProtoc.4741.

48. Lindau, M., and Fernandez, J.M. (1986). A patch-clamp study of histamine-secreting cells. J. Gen. Physiol. *88*, 349–368. https://doi.org/10.1085/jgp.88.3.349.

49. Biglari, N., Gaziano, I., Schumacher, J., Radermacher, J., Paeger, L., Klemm, P., Chen, W., Corneliussen, S., Wunderlich, C.M., Sue, M., et al. (2021). Functionally distinct POMC-expressing neuron subpopulations in hypothalamus revealed by intersectional targeting. Nat. Neurosci. *24*, 913–929. https://doi.org/10.1038/s41593-021-00854-0.

STAR★METHODS

KEY RESOURCES TABLE

REAGENT or RESOURCE	SOURCE	IDENTIFIER
Bacterial and virus strains		
AAV9-hSyn-DIO-hM4D(Gi)-mCherry	Addgene[41]	Addgene Cat# 44362-AAV9
pAAV-EF1a-double floxed-hChR2(H134R)-EYFP-WPRE-HGHpA (AAV1)	Addgene	Addgene Cat# 20298-AAV1
AAV1.Syn.Flex.GCaMP6s.WPRE.SV40	Addgene[42]	Addgene Cat# 100833-AAV1
AAV1 hSyn Flex-TVA-P2A-GFP-2A-oG GFP	Charité, Universitätsmedizin Berlin	BA-096
pSADB19dG-mCherry	Charité, Universitätsmedizin Berlin	BRABV-001
Chemicals, peptides, and recombinant proteins		
Buprenorphine	Bayer	PZN 01498870
Meloxicam	Boerhinger Ingelheim	PZN 07578423
6-cyano-7-nitroquinoxaline-2,3-dione (CNQX)	Sigma Aldrich/Merck	Cat# C127
DL-2-amino-5-phosphonopentanoic acid (DL-AP5)	Biotrend	Cat# BN0086
Picrotoxin	Sigma Aldrich/Merck	Cat# P1675
Bicuculline methiodide	Sigma Aldrich/Merck	Cat# 14343
Amphotericin B	Sigma Aldrich/Merck	Cat# A4888
D-Mannitol	AppliChem	Cat# A4831
20% glucose	DeltaSelect	N/A
Ensure Vanilla	Abbott, 400 g	N/A
Clozapine *N*-oxide (CNO)	Abcam	Cat#141704
RNAscope hydrogen peroxide	ACD bio / Bio-Techne	Cat#322381
RNAscope Protease Plus	ACD bio / Bio-Techne	Cat#322331
Opal 520 Fluorophore	Akoya Bioscience	Cat# FP1487001KT
Opal 570 Fluorophore	Akoya Bioscience	Cat# FP1488001KT
Opal 650 Fluorophore	Akoya Bioscience	Cat# FP1496001KT
Opal 690 Fluorophore	Akoya Bioscience	Cat# FP1497001KT
Critical commercial assays		
RNAscope Multiplex Fluorescent Reagent Kit v2	ACD bio / Bio-Techne	Cat#323100
RNAscope *Pnoc* probe	ACD bio / Bio-Techne	Cat#437881
RNAscope *Fos* probe	ACD bio / Bio-Techne	Cat#316921
RNAscope *Crabp1* probe	ACD bio / Bio-Techne	Cat#474711
RNAscope *Cre* probe	ACD bio / Bio-Techne	Cat#312281
RNAscope Neg control probe	ACD bio / Bio-Techne	Cat#321831
RNAscope Pos control probe	ACD bio / Bio-Techne	Cat#310771
Experimental models: Organisms/strains		
C57BL/6N	Charles River	Strain Code: 027
PNOC-Cre	Jais et al.[16]	N/A
B6.FVB-Tg(pnoc-EGFP)Uze	Zeilhofer HU, University of Zurich	N/A
POMC^{GFP} [C57BL/6J-Tg(Pomc-EGFP)1Low/J]	Jackson Laboratory	Stock number: 009593
Software and algorithms		
Fiji/ImageJ software	Schindelin et al.[43]	https://imagej.net/software/fiji/
GraphPad Prism (Version 9.1.0)	GraphPad Software Inc.	https://www.graphpad.com/scientific-software/prism/
R Studio	The R Foundation for Statistical Computing, Institute for Statistics and Mathematics, University of Economics and Business, Austria	https://www.r-project.org

(*Continued on next page*)

Continued

REAGENT or RESOURCE	SOURCE	IDENTIFIER
Patchmaster	HEKA	https://www.heka.com
pClamp/Clampfit	Molecular Devices	https://www.moleculardevices.com/
ExpeData	Sable Systems	https://www.sablesys.com
Spike2	Cambridge Electronic Design	http://ced.co.uk/
WinEDR	Strathclyde Electrophysiology Software	https://spider.science.strath.ac.uk/sipbs/software_ses.htm
Biorender	Biorender	https://biorender.com/
Inscopix Data Acquisition Software	Inscopix	Version 1.6.0
CNMF-E	Giovannucci et al.[44]	N/A
Github Repository	This study	https://github.com/bruening-lab/gabaergic_disinhibition_bnst_pnocarc_hfd_hyperphagia
Zenodo DOI	This study	https://zenodo.org/doi/10.5281/zenodo.10931409
Other		
Normal Chow Diet (ssniff R/M-H Phytoestrogenarm)	Ssniff Spezialdiäten	Cat# V1554
High-Fat Diet (ssniff, DIO)	Ssniff Spezialdiäten	Cat# EF D12492-(I)
Leica TCS SP-8-X Confocal microscope	Leica Microsystems	https://www.leica-microsystems.com/products/confocal-microscopes/p/leica-tcs-sp8-x/
Laser Diode Fiber Light Source (473 nM)	Doric Lenses	LDFLS_473/070
Mono Fiber-optic Patch Cords (200 μM – NA0.48)	Doric Lenses	MFP_200/230/900- 0.48_0.32m_FC-CM3(P)
SuperFrost Plus Gold slides	Thermo Fisher	Cat# K5800AMNT72
Vectashield Antifade Mounting Medium with DAPI	Vector Laboratories	Cat# H-1200
Metabond Quick Adhesive Cement System	Parkell	SKU: S380
GRIN lens 7.3mm length, NA 0.5	Inscopix	1050-004413
nVista System	Inscopix	N/A
Phenotyper	Noldus	N/A
Promethion core	Sable Systems	N/A
Vascular access buttons	Instech Laboratories	VABR1B/25

RESOURCE AVAILABILITY

Lead contact

Further information and requests for resources and reagents should be directed to and will be fulfilled by the lead contact, Jens Claus Brüning (bruening@sf.mpg.de).

Materials availability

No unique reagents were generated in this study.

Data and code availability

- All data reported in this paper will be shared by the lead contact upon request.
- All original code has been deposited at https://github.com/bruening-lab/gabaergic_disinhibition_bnst_pnocarc_hfd_hyperphagia, https://zenodo.org/records/10931410 and is publicly available as of the date of publication. DOIs are listed in the key resources table.
- Any additional information required to reanalyze the data reported in this paper is available from the lead contact upon request.

EXPERIMENTAL MODEL AND STUDY PARTICIPANT DETAILS

Animal welfare

All animal procedures were conducted in compliance with protocols approved by the local authorities (Bezirksregierung Köln). Permission to maintain, breed and use experimental mice was issued by the Department for Environment and Consumer

Protection - Veterinary Section, Cologne, North Rhine-Westphalia, Germany [(§11) 576.1.35.2.G 07/18, 81-02.04.2018.A087]. Mice were housed in individually ventilated cages at 22°C–24°C with 12-hour light/12-hour dark cycle and *ad libitum* access to water and food. Mice were single-housed to measure indirect calorimetry (Promethion, Sable Systems). All *in vivo* experiments were performed in adult males and females over 8 weeks of age.

Mouse lines

C57BL/6N - This mouse line was obtained from Charles River, France. PNOC-Cre – This mouse was generated in house and carries the Cre allele in exon 2 of the *Pnoc* gene.[16] Mice homozygous for the Cre allele lack the *Pnoc* gene product (PNOC Cre/Cre). PNOC-eGFP – BAC-transgenic *PNOC-eGFP* mice (B6.FVB-Tg(pnoc-EGFP)Uze, MGI:5426015) carrying an eGFP expression cassette introduced into the start codon of BAC RPCI 452H11 were used for electrophysiology experiments.

POMC-eGFP –. BAC-transgenic POMC-eGFP mice ($POMC^{GFP}$ [C57BL/6J-Tg(Pomc-EGFP)1Low/J]) were obtained from Jackson Laboratory (stock number: 009593) and described previously.[26]

For optogenetic stimulation of $PNOC^{ARC}$ neurons with and without nociceptin release, *PNOC-Cre* heterozygous mice were intercrossed.

For CRACM experiments, *PNOC-Cre* mice were crossed with *POMC-eGFP* mice or with *PNOC-eGFP* mice.

Animal diets

All mice were given *ad libitum* access to NCD (ssniff Spezialdiäten, catalog V1554-703) with a nutrient distribution of 67% of calories from carbohydrate, 23% from protein and 10% from fat. 3 Day high fat diet (3dHFD) refers to 3 days access to a diet with a nutrient distribution of 20% of calories from carbohydrate, 20% from protein and 60% from fat (ssniff Spezialdiäten; catalog E15742-350). Food restriction only occurred for limited time durations specific to the experiment: 16 hrs for fast-refeeding miniscope imaging; 8 hrs prior to gastric infusion and 1 hour before perfusion with optogenetic stimulation.

METHOD DETAILS

Stereotactic surgical procedures

For all stereotactic surgeries, adult animals (>20 g body weight, > 8 weeks of age) were anesthetized with isoflurane. The operations were performed on a warming blanket linked to a rectal thermometer and an eye and nose ointment (Bepanthen, Bayer) was applied to the eyes. After both shaving and disinfecting the skull region with octenisept (Schülke & Mayr GmbH) to keep the surgery under aseptic conditions, the mouse was fixed into a stereotactic apparatus (David Kopf Instruments) to determine the stereotactic coordinates using the mouse reference atlas from Paxinos and Franklin (Paxinos and Franklin, 2004). Following this, the skull surface was exposed through a skin incision, and a small drill hole was made. For pain relief and postoperative care, mice received buprenorphine (0.1 mg/kg) and meloxicam (5 mg/kg). Two days pre- and three days post-surgery, animals received analgesic treatment and they were monitored to ensure regain of pre-surgery body weight.

Miniscope experiments and mouse preparation

Virus delivery

To target the arcuate nucleus, 500 nL of pAAV.Syn.Flex.GCaMP6s.WPRE.SV40 (Addgene 100845-AAV1) with a titer of 5×10^{12} vg/ml was injected into the hypothalamus using the coordinates AP -1.45; ML -0.2; DV -5.85. The virus was injected using a borosilicate glass capillary (Drummond Scientific Company, 1-5 μL calibrated pipette) at a speed of 50 nl/min and was given 10 minutes to disperse.

GRIN-lens placement

Three weeks post virus injection, intracranial placement of a straight cuffed GRIN (GRadient INdex) lens (0.5 NA, 1/2 pitch, 0.6 x 7.3 mm, Inscopix Palo Alto, CA, USA) was implanted under isoflurane anesthesia. After skin removal, the skull was treated with a dental etching gel for roughening the cranial calotte (Super-Bond-C&B kit, Sun Medical Co., LTD, Japan) to improve the adhesion of the dental cement. To place the GRIN lens above the arcuate nucleus the following coordinates were used: AP -0.48; ML -0.3 and DV coordinates depended on each animal's GCAMP6s increase of fluorescence when inserting the implant (final position between 5.50 and 5.67). The stereotaxic arm was positioned at a -8° angle. To reduce intracranial pressure, before implanting the lenses, a blunt needle (diameter 0.5 mm) was inserted as follows (at DV (mm): number of steps (1 minute each)): -1: 2, -2: 4; -3: 5; -4:10; final DV: -4.9), (total time 30 minutes), after which the needle was removed. For lens implantation, the procedure followed the following time course: (at DV (mm): number of steps (1 minute each)): -1: 2, -2: 4; -3: 5; -4:10; -5.5: 5 (total time 35 minutes). The GRIN lens was fixed to the skull using MetaBond adhesive cement (Parkwell S380). The cut edges of the skin were sealed with 3M™ Vetbond™ Animal Tissue Adhesive (#1469, 3M Deutschland GmbH) to prophylactically prevent drying of these areas and possible skin infections. Four weeks after lens implantation surgery, mice were again anaesthetized, and a baseplate (Inscopix 100-000279, Inscopix 100-000241) was placed above the lens. The baseplate was fixed with MetaBond adhesive cement. To visualize GCaMP6s expression, light-emitting diode (LED)-driven excitation (1.2 mW/mm^2) was used with a wavelength of 475/10 nm. The emitted light (approx. 535/50 nm, green) was detected by the epifluorescence miniscope.

Gastric catheter cannulation

Gastric catheters were implanted as previously described.[45] Briefly, buprenorphine (0.1 mg/kg) was given intraperitoneally for analgesia 30 minutes before the procedure. Mice were then deeply anesthetized with 4-5% isoflurane and kept under deep anesthesia with 2-3% isoflurane. Midline incisions were placed in the skin, dorsally from the skull to the intrascapular region, and ventrally from the sternum about 1 cm towards the mid-abdomen. Next, the peritoneum was opened, the stomach was exposed with blunt forceps and the stomach wall of the greater curvature was punctured with jewellers-forceps. A 25ga polyurethane catheter (Instech Laboratories, Plymouth, UK) was inserted into the opening and secured to the stomach wall with a purse string using 5-0 silk (Silkam, Braun, Melsungen, Germany). The catheter was placed through a small incision in the muscle of the right flank and anchored to the muscle tissue with 4-0 silk (Silkam, Braun, Melsungen, Germany). The catheter was then placed into the previously prepared subcutaneous tunnel to exit the skin in the neck, and the peritoneum was closed using 4-0 silk. The open end of the catheter was attached to the vascular access button (Instech Laboratories, Plymouth, UK) in the neck, and skin incisions were closed with 4-0 silk in an interrupted suturing pattern. Catheters were rinsed through the access button twice weekly with sterilized drinking water.

Single neuron imaging

Before the experiment, mice were trained for 5 consecutive days with a dummy camera. The mice were kept in their home cage while recording their behavior with the Phenotyper system (Noldus). For refeeding experiments, mice were fasted overnight (5 PM until 9 AM) for 16 hours. For fasting experiments with gastric infusion, mice were moved to a new cage without food for an 8-hour period overnight (10 PM until 6 AM). This shorter fasting period is essential as infusion of content directly into the stomach of a mouse fasted for longer can harm the mouse and lead to death (unpublished observations). For intragastric infusions, an injector pumped Vanilla Ensure at a rate of 50 μL/min up to a total volume of 1.2 mL, providing 2.4 kcal, through a gastric cannula. After a 10-minute baseline recording, we recorded for 1 minute every 4 minutes during the total infusion period (31 minutes) and another 10 minutes post infusion. To record changes in the fluorescence intensity of GCaMP in $PNOC^{ARC}$ neurons, an excitation wavelength of 475/10 nm was used. Emitted light at a wavelength of 535/50 nm was recorded by the camera using following setup: 17 frames per second (fps) for all recordings, 6 to 7 gain intensity and 15-20% LED power. As the field of view (FOV) changes during the recording, post-mortem identification of $PNOC^{ARC}$ neurons was key to assure reliable data extraction (Figure S3).

Inscopix data analysis

For data preparation videos were preprocessed and motion corrected with IDPS (Inscopix Data Processing Software) and saved as .tiff files. Extraction of single cell data was obtained with CaImAn (Calcium Imaging Analysis), a Python toolbox and open-source library for large-scale calcium imaging data analysis.[44] With CaImAn, we employed the Constrained Nonnegative Matrix Factorization for micro-Endoscopic data (CNMF-E) algorithm on tiff neuronal videos for automatic neuronal activity identification and registration across different sessions of data collection. Accepted components suggested by the CNMF-E algorithm, neurons and their corresponding traces were extracted from the output, where each trace represented the activity of a neuron over a specific time period. Registration between videos was performed manually. We used an R script to further filter the accepted components provided by CaImAn with neurons matching IDPS FOV with the postmortem tissue of cells restricted to the ARC (detailed explanation in Figure S3). The lenses used had a 7.3 mm length with a 1.5 pitch, which rotates the IDPS image by 180° with respect to the correct anatomical orientation. All sections were collected using a cryostat (50 μm thickness), imaged using confocal microscopy and later analysed with IDPS FOV. Identification of the same neurons in the FOV of the first and last experiment confirmed GCaMP6s expression stability over time, and ruled out neuronal damage or cellular death due to GCaMP6s expression or imaging that could affect our behavioral experiments. Per experiment, neuronal traces were exported as .csv files for subsequent clustering analysis, *Z* score calculation and visualization.

Neuronal clustering and statistical analysis

Normalization and Z score calculation

To facilitate meaningful comparisons between neuron traces, a normalization process was carried out. For each neuron, a *Z* score was computed based on the mean and standard deviation of its baseline activity period (pre-intervention). This *Z* score transformation standardized each neuron's activity relative to its own baseline.

Clustering of neurons

The *Z* scored traces of neurons underwent a clustering process. Cosine dissimilarity was used as the distance metric to measure the angular difference between *Z* scored traces. The K-means clustering algorithm was applied with a predetermined value of k = 3, resulting in the classification of neurons into three distinct clusters based on their response to the intervention:

cluster 1 (UP): Neurons with increased signal compared to baseline; cluster 2 (NON): Neurons with unchanged signal relative to baseline; cluster 3 (DOWN): Neurons with reduced signal compared to baseline.

Optogenetic stimulation of $PNOC^{ARC}$ neurons

Surgeries

To express ChR2 in $PNOC^{ARC}$ neurons, 100 nL pAAV-EF1a-double floxed-hChR2(H134R)-EYFP-WPRE-HGHpA (AAV1, AAV1, 7×10^{12} vg/mL titer) was injected unilaterally (AP: -1.50, ML: 0.3, DV: 5.85-5.80) in PNOC-Cre/+ (heterozygous control) and PNOC Cre/Cre (homozygous PNOC knock-out) mice followed by an optical fiber implantation above the ARC (fiber core = 200 mm,

NA = 0.48, flat tip; Doric Lenses Inc.) coordinates from bregma AP: -1.5 mm DV: -5.4 ML: 0) and fixed to the skull using dental cement. The location of the fiber tip was histologically identified post mortem. Mice with missed virus injection or fiber placement outside of the target region were excluded from analysis.

In vivo optogenetic studies

One week prior to measurements, mice expressing ChR2 in $PNOC^{ARC}$ neurons were single-housed for acclimatization in metabolic cages, trained on attachment to an optic cable and were handled daily. For the experiment, recording started 1 hour before dark phase, and data was acquired over a 24-hour period with *ad libitum* access to NCD and water. Optogenetic stimulation was induced using a blue laser (474 nm) according to the following protocol: 5 ms pulses of 20 Hz; 1 s ON, 3 s OFF;15 mW output power.

Indirect calorimetry

Indirect calorimetry of optogenetically stimulated mice was performed using an indirect calorimetry system (Promethion, Sable Systems) of mice aged 12-17 weeks. Mice were acclimatized to their cages and patch cords for 1 week prior to experiments. 1 hour prior to the recording period, mice were attached to the patch cord. Recording started at the onset of the dark cycle for a 16-hour time period, once with the laser ON (20 Hz, 5 ms pulses, 1s ON-3s OFF) and once with the laser OFF. Raw data were analyzed using the software ExpeData v.1.9.22 and Sable Systems Macro Interpreter v2.38 (Promethion, Sable Systems) via an analysis script with 10-minute data binning.

Electrophysiological recordings

Brain slice preparation

Animals were anesthetized with isoflurane, decapitated, and coronal brain slices (250-300 μm) containing the ARC were cut with a vibratome. For perforated patch recordings, the brains were sliced and submerged in cold (4°C), carbonated (95% O_2 and 5% CO_2), glycerol-based modified artificial cerebrospinal fluid (GaCSF).[46] GaCSF contained (in mM): 244 glycerol, 2.5 KCl, 2 $MgCl_2$, 2 $CaCl_2$, 1.2 NaH_2PO_4, 10 HEPES, 21 $NaHCO_3$, and 5 glucose, adjusted to pH 7.2 with NaOH. For spontaneous and light-evoked postsynaptic current recordings, brains were sliced and submerged in ice-cold cutting solution consisting of (in mM): 92 choline chloride, $NaHCO_3$, 25 Glucose, 20 HEPES, 10 $MgSO_4$, 2.5 KCl, 1.25 NaH_2PO_4, 5 sodium ascorbate, 3 sodium pyruvate, 2 thiourea, 0.5 $CaCl_2$; oxygenated with 95% O2/5% CO2; measured osmolarity 310–320 mOsm/L. Afterwards, slices were transferred into carbonated aCSF at 36°C for 30-40 minutes and then kept at room temperature until further usage for electrophysiological recordings. aCSF contained: (in mM) 125 NaCl, 2.5 KCl, 2 $MgCl_2$, 2 $CaCl_2$, 1.2 NaH_2PO_4, 21 $NaHCO_3$, 10 HEPES, and 5 glucose, adjusted to pH 7.2 with NaOH. Brain slices were continuously superfused during electrophysiological recordings with carbonated (95% O_2; 5% CO_2) aCSF at a flow rate of ~2.5 ml·min^{-1}. In all recordings, the aCSF contained 5 × 10^{-5} M DL-AP5 (BN0086, Biotrend) and 10^{-5} M CNQX (C127, Sigma-Aldrich) to block glutamatergic synaptic transmission. The aCSF for the perforated patch recordings investigating the nociceptin effect additionally contained 10^{-4} M picrotoxin (P1675, Sigma-Aldrich) and 5 x 10^{-6} M CGP-54626 (BN0597 Biotrend) to block GABAergic synaptic transmission.

sIPSC and sEPSC recordings

Experiments were performed on brain slices from 8-12 weeks-old male and female mice either fed NCD or 3dHFD prior to the experiment. To visualize PNOC neurons in the ARC, we used a *PNOC-eGFP* line that expressed enhanced green fluorescent protein (eGFP) selectively in PNOC neurons. For recording of sIPSCs, borosilicate glass microelectrodes (3-5 MΩ) were filled with a CsCl-based internal solution consisting of (in mM): 140 CsCl, 2 NaCl, 10 HEPES, 5 EGTA, 2 $MgCl_2$, 0.5 $CaCl_2$, 2 Na_2-ATP, 0.5 Na_2-GTP, 2 QX-314, pH of 7.3 with CsOH. For sEPSC recordings, a $CsMeSO_3$-based internal solution consisting of (in mM): 135 $CsMeSO_3$, 10 HEPES, 1 EGTA, 4 $MgCl_2$, 4 Na2-ATP, 0.4 Na_2-GTP, 10 Na_2-phosphocreatine (pH 7.3 adjusted with CsOH; 295 mOsm/L) was used. Recordings were performed at a holding potential of V_h = -70 mV. All recordings were made using a Multiclamp 700B amplifier, data were filtered at 2 kHz and digitized at 10 kHz. sIPSC and sEPSC frequency and mean peak amplitude were determined using WinEDR (version 3.8.6). Recordings with a series resistance (R_s) change of > 20% were discarded from analysis.

Recordings of light-evoked-IPSCs

PNOC-eGFP and *PNOC-Cre::PNOC-eGFP* mice were unilaterally injected with pAAV-hSyn-hChR2(H134R)-EYFP (AAV1, 150 nL of 1×10^{13} vg/mL titer) and pAAV-EF1a-double floxed-hChR2(H134R)-EYFP-WPRE-HGHpA (AAV1, 50 nL of 7×10^{12} vg/mL titer) in the BNST. 3 weeks post-surgery, brain slices were prepared as outlined above. Borosilicate glass microelectrodes (3-5 MΩ) were filled with the CsCl-based internal solution as described above. To photostimulate ChR2-expressing terminals, an LED light source (473 nm) was focused onto the back aperture of the microscope objective, producing widefield exposure around recorded cells. le-IPSCs were recorded from eGFP-positive ARC neurons in whole-cell voltage-clamp mode, with the membrane potential clamped at Vh = -70 mV, for determining connectivity between BNST neurons and $PNOC^{ARC}$ neurons. At the end of the recordings, bicuculline (10 mM) was added to the aCSF to verify the GABAergic nature of the recorded currents. The le-IPSC detection protocol consisted of four blue light pulses (473 nm wavelength, 5 ms) administered 1 s apart during the first 4 s of a 10s sweep. le-IPSCs with short latency (< 10 ms) upon light stimulation and low jitter were considered light-driven. Further characterization of synaptic parameters was obtained by applying a pair of light stimuli 150 ms apart while recording light-evoked IPSCs at $V_h = -70$ mV. Paired pulse ratios (PPRs) were determined by dividing the amplitude of the second le-IPSC by the amplitude of the first le-IPSC averaged over 10 sweeps. To determine the size of the le-IPSC, we compared the peak current size of the first le-IPSC between groups. asynch-leIPSCs recorded in strontium-containing-aCSF (in mM): 126 NaCl, 21.4 $NaHCO_3$, 2.5 KCl, 1.2 NaH_2PO_4, 1 $MgCl_2$, 5 Sr^{2+}, 10 glucose. asynch-leIPSCs

were manually detected in a time window of 300 ms after the 5ms light pulse. Light output was controlled by a programmable pulse stimulator, Master-8 (A.M.P.I.) and pClamp software (Axon Instruments). All recordings were analyzed offline using Clampfit.

sIPSCs in POMC neurons

PNOC-Cre::POMC-eGFP mice were injected unilaterally with pAAV-hSyn-DIO-hM4D(Gi)-mCherry (AAV9, 50 nl, 100 nL of 7×10^{12} vg/mL titer) in the ARC and given 3 weeks for the virus to express. Three days prior to the experiment, the mice either continued to be fed a NCD or switched to 3dHFD. Brain slices were prepared as outlined above and sIPSCs recordings from POMC neurons were obtained in voltage-clamp mode at V_h = -70 mV. To determine the direct effects of $PNOC^{ARC}$ neuron inhibition, recordings were performed in normal aCSF or in aCSF supplemented with CNO (10 μM). In addition, for paired recordings, CNO (10 μM) was added to the circulating aCSF after a 5 min baseline recording. Recordings with a R_s change of > 20% were discarded from analysis. sIPSC frequency and mean peak amplitude were determined using WinEDR (version 3.8.6) for a period of 3 minutes for each recording and was manually inspected.

Perforated patch clamp recordings

To investigate the nociceptin effect on POMC neurons, perforated patch clamp recordings under current or voltage clamp were performed at ~32°C as described previously.[47] Neurons were visualized with a fixed-stage upright microscope (BX51WI, Olympus) using an ×40 or ×60 water-immersion objective (LUMplan FL/N ×40, 0.8 numerical aperture, 2 mm working distance; LUMplan FL/N × 60, 1.0 numerical aperture, 2 mm working distance, Olympus) equipped with fluorescence optics and infrared differential interference contrast optics. Neurons were identified by their anatomical location in the ARC and by their eGFP fluorescence. Electrodes with tip resistances between 4 and 7 MΩ were fashioned from borosilicate glass (0.86-mm inner diameter; 1.5-mm outer diameter; GB150-8P, Science Products) with a vertical pipette puller (PP-830, Narishige). All recordings were performed with an EPC10 patch-clamp amplifier (HEKA) controlled by the program PatchMaster (version 2x90; HEKA) running under Windows. In parallel, data were recorded using a micro1410 data acquisition interface and Spike 2 (version 7.01, both from CED). Current clamp recordings were sampled at 25 kHz and low-pass filtered at 2 kHz with a four-pole Bessel filter. The calculated liquid junction potential of 14.6 mV between intracellular and extracellular solution was compensated (calculated with Patcher's Power Tools plug-in from https://www3.mpibpc.mpg.de/groups/neher/index.php?page=software for IGOR Pro 6; Wavemetrics). The perforated patch experiments were carried out using protocols that were modified from previous studies, as summarized in.[47] Recordings were performed with a pipette solution containing (in mM): 140 K-gluconate, 10 KCl, 10 HEPES, 0.1 EGTA, and 2 $MgCl_2$, adjusted to pH 7.2 with KOH. ATP and GTP were omitted from the intracellular solution to prevent uncontrolled permeabilization of the cell membrane.[48] The patch pipette tip was filled with intracellular solution and backfilled with intracellular solution, which contained the ionophore amphotericin B (A4888, Sigma-Aldrich) to achieve perforated patch recordings, 0.02% tetramethylrhodamine-dextran (D3308, Invitrogen) to monitor the stability of the perforated membrane and 1% biocytin (B4261, Sigma-Aldrich) to label the recorded neuron. Amphotericin B was dissolved in DMSO to a concentration of 40 μg/μl (D8418, Sigma-Aldrich). The ionophore was added to the modified pipette solution shortly before use. The final concentration of amphotericin B was ~120–160 μg/ml. Amphotericin solutions were prepared from undissolved weighted samples (stored at 4°C and protected from light) every recording day. During the perforation process, the spike amplitude and R_s was monitored, and experiments started after the action potential amplitude and R_s values were stable (~10–20 min). A change to the whole-cell configuration was indicated by 'rhodamine-fluorescence' in the cell body. To investigate the nociceptin responses in POMC neurons of *POMC-eGFP* mice, increasing nociceptin (0910, Tocris) concentrations were sequentially bath-applied 10 min for each concentration. The concentrations of 1 nM, 10 nM, 100 nM, and 500 nM were applied in current clamp recordings, and the concentrations 1 nM, 3 nM, 6 nM, 10 nM, 50 nM, and 100 nM were applied in voltage clamp recordings. Data analysis was performed with Spike2 (Cambridge Electronics), GraphPad Prism (version 5.04 and 8.4.3; GraphPad Software Inc), and custom-made analysis scripts written in Igor Pro. The numerical values are given as mean ± SEM. The concentration-response relation was fit with a 'sigmoidal dose-response fit' of the form $y = Bottom + (Top - Bottom)/1 + 10^{logEC50-X}$.

Monosynaptic rabies tracing of $PNOC^{ARC}$ neurons

Viruses and surgeries

Heterozygous *PNOC-Cre* mice were injected with 10 nL (10^8 vp/ml) of AAV-hSyn-Flex-TVA-P2A-GFP-2A-oG GFP (AAV1, catalog item BA-096, Charité) into the ARC. Three weeks later, mice received an injection of 25 nL (10^9 vp/ml) of EnvA G-deleted Rabies virus coding for mCherry (pSADB19dG-mCherry; catalog item #BRABV-001, Charité) into the ARC.

Histology

Mice were deeply anesthetized by *i.p.* injection of ketamine and xylazine (Body weight (BW) <35g: 100mg/kg BW ketamine and 18 mg/kg BW xylazine; BW >35g: 120 mg/kg BW ketamine und 18 mg/kg BW xylazine), and then transcardially perfused with 0.9% saline followed by 4% paraformaldehyde (PFA) in PBS. After post-fixation overnight, brains were isolated and moved to 20% sucrose (in PBS) for 2 days. For imaging and analysis, whole brains were coated with tissue freezing medium and coronal sections (20 μm thick) were prepared on a cryostat (Leica CM1900).

Imaging and data analysis

Whole brain sections were imaged with an automated slide scanner (VS120 Virtual Slide, Olympus) or a confocal microscope (SP-8 Leica, equipped with HCX-PL Fluotar × 10 (0.3 NA), HC PL APO ×20 (0.75 NA). The locations of the labelled neurons and outlines of the brain nuclei were manually counted according to the mouse brain atlas (Paxinos and Franklin, 2001). Brightness, contrast and pseudocolor were adjusted, as needed, using ImageJ (NIH).

RNA *in situ* hybridization (ISH)

The fluorescence ISH technique (RNAscope, ACDbio) was used to detect mRNA of *Pnoc, Crabp1*, *Cre*, and *Fos*. All reagents were purchased from Advanced Cell Diagnostics (ACD) and protocols followed according to the manufacturer's instructions or according to modified protocols.[49] Following probes were used: *Pnoc* (ACD, Cat. No. 437881), *Crabp1* (ACD, Cat. No. 474711), *Cre* (ACD, Cat. No. 312281), and *Fos* (ACD, Cat. No. 316921). Negative (ACD, Cat. No. 321831) and positive-control probes (ACD, Cat. No. 310771) were processed in parallel with the target probes. The probes were detected using tyramide-diluted Opal570 (1:1,000 dilution), Opal620 (1:1,000 dilution) and Opal690 (1:1,000 dilution). Sections were counterstained with DAPI and mounted with ProLong Gold Antifade Mountant (Thermo Fisher, P36931), and stored at 4 °C in dark. Images were captured using a confocal Leica TCS SP-8-X microscope, equipped with a ×40/1.30 oil objective. Z-stacks were taken with optical sections of 1 μm. Laser intensities were kept constant throughout all related conditions. Images were imported into FIJI (National Institutes of Health, version 2.0.0-rc-41/1.50d) and quantified by targeting ROI along the Z-stack and confirming in the maximal projection image. A positive counted cell had 4 or more fluorescent dots around the nuclei.

QUANTIFICATION AND STATISTICAL ANALYSIS

The number of replicates (*n*) are indicated in the figure legends. For electrophysiology experiments, *n* represents the number of recorded neurons. Data are presented as Box-whisker plots or as violin plots with mean (red dot), minimum and maximum values. For all statistical tests, significance was measured against an alpha value of 0.05. ns, not significant, $*p < 0.05$, $**p < 0.01$, $***p < 0.001$, $****p < 0.0001$. All error bars show the standard error of the mean (SEM). No statistical methods were used to predetermine sample sizes, but group sizes commonly applied in rodent studies were used. All statistical analyses were performed using GraphPad Prism software unless noted otherwise. Electrophysiology analysis was performed with Spike2 (version 7; Cambridge Electronic Design Ltd., Cambridge, UK), Igor Pro 6 (Wavemetrics, Portland, OR, USA), WinEDR (version 3.8.6, Strathclyde Electrophysiology Software), Clampfit (version 10.7) and Graphpad Prism (version 5.0b; version 10; Graphpad Software Inc., La Jolla, CA, USA). If not stated otherwise, all calculated values are expressed as mean +/- SEM. For pairwise comparisons of independent, not normal distributions Mann-Whitney U-test was used. For pairwise comparisons of dependent and independent normal distributions without predictions paired and unpaired two-tailed t tests were used, and a one-tailed t-test was used for pairwise comparisons with predictions. To compare changes in proportions of neuronal responses a chi-square test was used. Tests were executed using GraphPad Prism 5 and 10 (GraphPad Software Inc., La Jolla, CA, USA). Neurons with action potential frequencies below 0.5 Hz were defined as silent. For Inscopix data analysis, a Welch's t-test was conducted on the mean *Z* scored traces comparing baseline and post-intervention. This analysis was performed in two ways: (i) For all neurons, identifying global changes resulting from the intervention. (ii) Separately for each cluster, identifying changes specific to each group. These methods provided a comprehensive understanding of the neuronal response to the intervention, allowing for the identification of clusters with varying levels of activity alteration.